

# Numerically “exact” charge transport dynamics in a dissipative electron–phonon model rationalizing the success of the transient localization scenario

Veljko Janković

*Institute of Physics Belgrade, University of Belgrade, Pregrevica 118, 11080 Belgrade, Serbia<sup>a)</sup>*

Optical conductivity in molecular semiconductors is suppressed in the terahertz region, featuring the displaced Drude peak that reflects carriers’ transient localization (TL) by slow intermolecular vibrations. Meanwhile, recent computations in minimal models evidence optical-conductivity enhancements below the characteristic vibrational frequency, which cannot be captured by the TL phenomenology. These models assume undamped vibrations, whereas atomistic simulations show that the vibrations most strongly modulating carrier’s hopping amplitude are damped. Here, we use the dissipaton equations of motion (DEOM) method to compute finite-temperature real-time current autocorrelation function in a one-dimensional model with Brownian-oscillator spectral density of nonlocal carrier–phonon interaction. We exploit the dissipaton algebra to handle the phonon-assisted current, reduce the method’s computational requirements by working in momentum space, and confirm that numerically stable transport dynamics are virtually independent of a specific DEOM closing scheme. With increasing damping, we find that DEOM optical-conductivity profiles become increasingly qualitatively similar to TL predictions. For parameters representative of room-temperature hole transport in single-crystal rubrene, we conclude that the TL phenomenology is established already in the underdamped-oscillator regime. Reasonable variations in the damping constant weakly affect the carrier mobility, which remains within experimental bounds. Overall, our results strongly suggest that optical-conductivity enhancements at very low frequencies are artifacts of undamped vibrations, and rationalize the success of the TL phenomenology in describing experimental data.

## I. INTRODUCTION

It is by now well established that the motion of a charge carrier in high-mobility organic semiconductors is mainly limited by its moderate coupling to slow and abundantly thermally excited intermolecular vibrations.<sup>1–7</sup> The carrier’s optical response then features a displaced Drude peak (DDP) in the terahertz region,<sup>8–13</sup> which can be reproduced by the phenomenological Drude–Anderson model<sup>3,14</sup> that rests on the TL scenario (TLS).<sup>3,15,16</sup> Starting from the frozen-phonon limit and introducing effective phonon dynamics in the relaxation-time approximation,<sup>3,15</sup> the TLS offers a physically plausible and computationally favorable alternative<sup>17,18</sup> to quantum-classical simulations of coupled carrier–phonon dynamics.<sup>1,19–21</sup> The latter are considered as the best available approximation to fully quantum dynamics, which are prohibitively expensive in the physically relevant slow-phonon regime.<sup>5,22,23</sup> This holds true even in the one-dimensional transport model featuring a single vibrational mode per lattice site.<sup>1,3</sup>

This state of affairs has changed very recently with us devising a numerically “exact” hierarchical equations of motion (HEOM)-based approach to carrier transport<sup>24,25</sup> in the above-described one-dimensional Peierls (or Su–Schrieffer–Heeger)<sup>26–28</sup> model. For model parameters appropriate for room-temperature hole transport along the maximum-conductivity direction in single crystals of

rubrene,<sup>23</sup> we evidence subtle qualitative differences between HEOM results and TLS predictions at long times (low frequencies). Namely, HEOM (TLS) shows that the diffusive transport is ultimately reached from the super-diffusive (sub-diffusive) side, with optical response increasing (decreasing) as  $\omega \rightarrow 0$ .<sup>25</sup> The results of the most recent quantum-classical approaches,<sup>21</sup> to which the HEOM method reduces in the slow-phonon limit, display long-time and low-frequency features that are fully compatible with our HEOM results. Meanwhile, most experimental low-frequency signatures align with TLS (Drude–Anderson) predictions,<sup>9–12</sup> though there are exceptions.<sup>8</sup>

The aforementioned minimal-model studies<sup>21,25</sup> assume that the carrier hopping amplitude is modulated by a single phonon mode (also known as the “killer” mode<sup>7,29</sup>) of frequency  $\omega_0 \approx 50 \text{ cm}^{-1}$ . Although the “killer” mode does have the dominant contribution to the total dynamic disorder, the remaining low-frequency vibrations, typically quasi-continuously distributed over the  $(0 - 200) \text{ cm}^{-1}$  range,<sup>30</sup> act as a thermal bath that effectively introduces friction to the “killer”-mode dynamics.<sup>30,31</sup> Indeed, molecular-dynamics simulations of crystalline rubrene<sup>23</sup> and a discotic liquid crystal<sup>30,32</sup> show that the most intensive Fourier component of the transfer-integral autocorrelation function corresponds to either underdamped<sup>23</sup> or overdamped<sup>30</sup> oscillations in the time domain. In other words, the spectral density (SD) of the carrier–phonon interaction,<sup>33,34</sup> which is the only phonon-dependent quantity determining purely carrier dynamics under standard assumptions,<sup>35</sup> can be reasonably described within the Brownian-oscillator (BO)

<sup>a)</sup> Electronic mail: veljko.jankovic@ipb.ac.rs

model.<sup>33,36,37</sup>

When approached from the perspective of open quantum dynamics,<sup>38,39</sup> phonon-limited charge transport is usually studied by tracking the relaxation of an initial nonequilibrium charge distribution towards equilibrium.<sup>40–44</sup> However, such approaches cannot access the time-dependent diffusion constant or frequency-dependent mobility,<sup>45,46</sup> which are related to the finite-temperature time-dependent current autocorrelation function.<sup>47,48</sup> Methods of open quantum dynamics have recently been used to compute autocorrelation function of the purely electronic current operator within the Holstein model.<sup>44–46,49–51</sup> Analogous computations for the Peierls model are difficult because one has to express the expectation values involving the phonon-assisted current<sup>49,52–54</sup> in terms of purely electronic quantities remaining upon integrating phonons out.

This problem can be solved within the DEOM framework,<sup>55–59</sup> which we employ here to study carrier transport dynamics in a dissipative Peierls model.<sup>21,30</sup> In contrast to most open quantum dynamics-based studies,<sup>40,42,44</sup> which employ the Drude–Lorentz (DL) SD to model the interaction of a carrier with low-frequency phonons,<sup>33</sup> we assume the more physically plausible<sup>60</sup> BO SD. We concentrate on model parameters representative of room-temperature hole transport along the maximum-conductivity direction in single crystals of rubrene.<sup>3,23</sup> We use the generalized Wick’s theorem<sup>55–59</sup> to handle the phonon-assisted current and circumvent potential long-time numerical instabilities<sup>61</sup> by applying an appropriate DEOM closing scheme,<sup>24,62</sup> which enables us to reliably access the diffusive dynamics and thus the low-frequency dynamical mobility.

For weakly damped phonons, subdiffusive carrier dynamics remain limited to intermediate timescales, similarly to our HEOM results at zero damping.<sup>25</sup> The diffusive transport is then approached from the superdiffusive side, giving rise to a dynamical-mobility enhancement below the phonon frequency. As the damping is increased, the diffusive transport sets in from the subdiffusive side, and DEOM results are qualitatively similar to TLS predictions and experimental results, which feature a steady dynamical-mobility suppression below the DDP. We find that this change in the character of the long-time dynamics and low-frequency optical response occur in the region of underdamped BO, at dampings such that the phonon frequency remains well defined. Physically reasonable variations in the damping constant weakly affect the dc mobility, which remains within experimental bounds. Our results provide strong evidence that the long-time superdiffusive dynamics and low-frequency dynamical-mobility enhancements reported in minimal models<sup>21,25</sup> are artifacts of the assumed undamped phonon dynamics.

The paper is organized as follows. Section II introduces the model and the DEOM formalism. Section III discusses some technical aspects necessary to obtain reliable DEOM results, which we present in Sec. IV. We

summarize our main conclusions in Sec. V.

## II. MODEL AND METHOD

### A. Model

We study phonon-limited carrier transport in a dissipative version of the one-dimensional model considered in Refs. 1, 3, 21, 24, and 25. The motion of a carrier along an  $N$ -site chain with periodic boundary conditions is affected by the interaction with a bath of harmonic oscillators, instead of  $N$  undamped oscillators considered in Refs. 1, 3, 21, 24, and 25. In the following, we set the elementary charge  $e_0$ , the lattice constant  $a_l$ , and physical constants  $\hbar$  and  $k_B$  to unity.

The total Hamiltonian in momentum space reads

$$H_{\text{tot}} = H_S + H_B + H_{S-B} \\ = \sum_k \varepsilon_k |k\rangle\langle k| + \sum_{q\xi} \omega_\xi b_{q\xi}^\dagger b_{q\xi} + \sum_q V_q B_q. \quad (1)$$

In Eq. (1), the wavenumbers of the carrier ( $k$ ) and bath oscillators ( $q$ ) can assume  $N$  allowed values  $\frac{2\pi n}{N} \in (-\pi, \pi]$ . The carrier Hamiltonian  $H_S$  describes a free-carrier band with dispersion  $\varepsilon_k = -2J \cos k$  originating from nearest-neighbor hops of amplitude  $J$ . The bath Hamiltonian  $H_B$  describes  $N$  identical sets of harmonic oscillators, which are associated with individual sites and counted by index  $\xi$ . The interaction Hamiltonian  $H_{S-B}$  depends on the carrier operator

$$V_q = \sum_k M(k, q) |k+q\rangle\langle k|, \quad (2)$$

with

$$M(k, q) = -2i [\sin(k+q) - \sin k], \quad (3)$$

and the bath operator (with  $\bar{q} = -q$ )

$$B_q = \sum_\xi \frac{g_\xi}{\sqrt{N}} (b_{q\xi} + b_{\bar{q}\xi}^\dagger). \quad (4)$$

The carrier–bath matrix element  $M(k, q)$  in Eq. (3) describes linear modulation of nearest-neighbor hopping amplitudes by the difference between displacements of the corresponding local oscillators<sup>1,3,28,63</sup> [see also Eq. (45)]. Equation (3) implies that bath modes with  $q = 0$  are uncoupled from the rest of the system. In the following, we understand that the  $q = 0$  term is omitted from all sums over phonon wave numbers.

### B. Spectral density of carrier–phonon interaction

In the model specified by Eq. (1), the influence of the bath on carrier dynamics is fully captured by the SD of

carrier–bath interaction

$$\mathcal{J}(\omega) = \pi \sum_{\xi} g_{\xi}^2 [\delta(\omega - \omega_{\xi}) - \delta(\omega + \omega_{\xi})]. \quad (5)$$

In models without explicit dissipation,<sup>1,3,21,24,25</sup>  $\mathcal{J}(\omega)$  consists of delta peaks at  $\pm\omega_0$ , where  $\omega_0$  is the frequency of the undamped vibrational mode. Here, we mainly consider the BO SD<sup>33,34,64,65</sup>

$$\mathcal{J}_{\text{BO}}(\omega) = 2E_0 \frac{\omega_0^2 \cdot 2\gamma_0\omega}{(\omega_0^2 - \omega^2)^2 + (2\gamma_0\omega)^2} \quad (6)$$

which, in the limit of zero damping  $\gamma_0$ , reduces to the delta-like SD studied in Refs. 1, 3, 21, 24, and 25. Microscopically, the damping can be traced back to the coupling of the undamped vibration to an Ohmic bath,<sup>36,37</sup> which can be considered to stem from the quasicontinuum of neglected low-frequency vibrational modes that typically span the  $(0 - 200) \text{ cm}^{-1}$  range.<sup>5,30</sup> The BO SD can thus be regarded as an effective SD modulating transitions between electronic states that is equivalent to the Ohmic SD modulating transitions between vibronic (mixed vibrational and electronic) states.<sup>66–68</sup> As the SD conveniently combines information on the carrier–phonon interaction strength and phonon density of states, see Eq. (5), the BO SD can be considered as a convenient model of the influence of a continuous (as opposed to the delta-like<sup>1,3,21,24,25</sup>) density of phonon states on carrier dynamics. The quantity

$$E_0 = \sum_{\xi} \frac{g_{\xi}^2}{\omega_{\xi}} = \int_{-\infty}^{+\infty} \frac{d\omega}{2\pi} \frac{\mathcal{J}_{\text{BO}}(\omega)}{\omega} \quad (7)$$

is one half of the zero-temperature polaron binding energy in the two-site version of this model, which is analytically solvable.<sup>27</sup> We then define the dimensionless carrier–phonon interaction constant as

$$\lambda = \frac{2E_0}{J}. \quad (8)$$

The BO is underdamped for  $\gamma_0 < \omega_0$ , critically damped for  $\gamma_0 = \omega_0$ , and overdamped for  $\gamma_0 > \omega_0$ . The changes in the BO SD and the so-called frictional spectrum  $\mathcal{J}_{\text{BO}}(\omega)/\omega$ <sup>69</sup> with  $\gamma_0$  are summarized in Figs. 1(a) and 1(b), respectively. The frictional spectrum, which essentially determines the free-bath propagator at high temperatures [Eq. (11) with  $\beta\omega \ll 1$  whenever  $\mathcal{J}_{\text{BO}}(\omega)$  is appreciable],<sup>31</sup> peaks at a non-zero (zero) frequency for  $\gamma_0 < \omega_0/\sqrt{2}$  ( $\gamma_0 \geq \omega_0/\sqrt{2}$ ).<sup>70</sup>

Many studies aiming at a fundamental understanding of carrier dynamics in organic semiconductors employ the DL SD<sup>40,42,44</sup>

$$\mathcal{J}_{\text{DL}}(\omega) = 2E_0 \frac{\omega\gamma_{\text{DL}}}{\omega^2 + \gamma_{\text{DL}}^2}, \quad (9)$$

where  $\gamma_{\text{DL}}$  is the characteristic bath frequency. In contrast to the high-frequency behavior  $\mathcal{J}_{\text{BO}}(\omega) \propto \omega^{-3}$  of

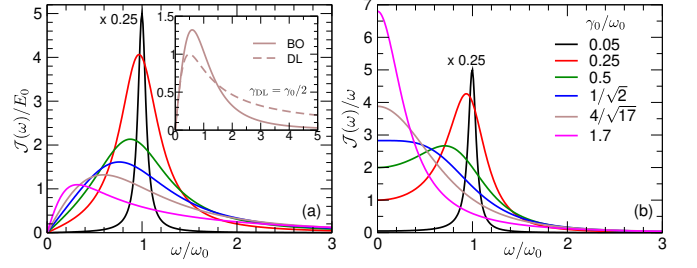


FIG. 1. Frequency profile of (a) the BO SD [Eq. (6)] and (b) the BO friction spectrum  $\mathcal{J}_{\text{BO}}(\omega)/\omega$  for different values of the damping  $\gamma_0$ . The curves for  $\gamma_0/\omega_0 = 0.05$  are scaled down by a factor of 4 for visual clarity. The inset in (a) compares the BO SD for  $\gamma_0/\omega_0 = 4/\sqrt{17}$  to the DL SD [Eq. (9)] with  $\gamma_{\text{DL}} = \gamma_0/2$ .

the BO SD, the DL SD exhibits a long high-frequency tail  $\mathcal{J}_{\text{DL}}(\omega) \propto \omega^{-1}$ . Therefore, even in the high-temperature regime  $2\pi T \gg \gamma_{\text{DL}}$ , to which the typically used values of  $\gamma_{\text{DL}} = 40 \text{ cm}^{-1}$  and  $T = 300 \text{ K} = 210 \text{ cm}^{-1}$  belong,<sup>40,42,44</sup> the long tail of the DL SD implies that HEOM/DEOM computations have to take into account a number of Matsubara terms to achieve full convergence.<sup>60</sup> To reduce that number, Ishizaki<sup>60</sup> proposed that the DL SD in Eq. (9) be replaced with the BO SD in Eq. (6) with  $\gamma_0 = 2\gamma_{\text{DL}}$  and  $\omega_0^2 = \gamma_0^2 + \epsilon^2$  with  $|\epsilon| \lesssim \gamma_0/4$ . The inset of Fig. 1(a) compares the DL SD to the corresponding BO SD for  $|\epsilon| = \gamma_0/4$ , so that  $\gamma_0/\omega_0 = 4/\sqrt{17}$ . In addition to lowering the number of Matsubara terms, Ishizaki's approximation to DL SD circumvents unphysical short-time dynamics of mixed carrier–phonon quantities, which we discuss in Sec. IV D.

### C. Dissipaton decomposition

The sole bath quantity influencing the reduced carrier dynamics is the free-bath propagator ( $t > 0$ )<sup>35</sup>

$$\langle B_{q_2}^{(I)}(t) B_{q_1}^{(I)}(0) \rangle_B = \frac{\delta_{q_1 q_2}}{N} \mathcal{C}(t), \quad (10)$$

where  $\langle \cdot \rangle_B$  denotes averaging over the equilibrium state  $\rho_B^{\text{eq}} = e^{-\beta H_B} / \text{Tr}_B e^{-\beta H_B}$  of the bath at temperature  $T = \beta^{-1}$ ,  $B_q^{(I)}(t) = e^{iH_B t} B_q e^{-iH_B t}$ , while

$$\mathcal{C}(t) = \int_{-\infty}^{+\infty} \frac{d\omega}{\pi} e^{-i\omega t} \frac{\mathcal{J}_{\text{BO}}(\omega)}{1 - e^{-\beta\omega}} \approx \sum_{m=0}^{K-1} c_m e^{-\mu_m t}. \quad (11)$$

The exponential decomposition of  $\mathcal{C}(t)$  involves a total of  $K = N_{\mathcal{J}} + N_{\text{BE}}$  terms,  $N_{\mathcal{J}}$  ( $N_{\text{BE}}$ ) of which stem from the poles of the BO SD (the Bose–Einstein factor) in the lower half plane (so that  $\text{Re} \mu_m > 0$ ). The coefficients  $c_m$  are in general complex, while the coefficients  $\mu_m$  appear either purely real or in complex-conjugated pairs,<sup>57</sup> which motivates the definition of index  $\bar{m}$  by  $\mu_{\bar{m}} = \mu_m^*$ . The values of  $c_m$  and  $\mu_m$  for the BO SD are summarized in Appendix A.

Equation (11) motivates the introduction of dissipaton operators<sup>57,59</sup>  $f_{qm}$  such that  $B_q \approx \sum_{m=0}^{K-1} f_{qm}$ , while

$$\left\langle f_{q_2 m_2}^{(I)}(t) f_{q_1 m_1}^{(I)}(0) \right\rangle_B = \delta_{m_1 \overline{m_2}} \eta_{q_2 q_1 m_2} e^{-\mu_{m_2} t}, \quad (12)$$

with  $\eta_{q_2 q_1 m} = \delta_{q_1 \overline{q_2}} c_m / N$ . Equation (12) somewhat differs from the standard DEOM prescription, which features  $\delta_{m_1 m_2}$  instead of  $\delta_{m_1 \overline{m_2}}$ , see, e.g., Eq. (3.2) of Ref. 57 or Eq. (8) of Ref. 59. Our choice in Eq. (12) is motivated by the requirement that the dissipative theory smoothly reduces to the dissipationless case as  $\gamma_0 \rightarrow 0$ . Then, we have demonstrated<sup>24</sup> that  $f_{qm}$  are proportional to the creation and annihilation operators  $b_q$  and  $b_q^\dagger$  of a single vibrational quantum. The same continuity argument implies that  $f_{qm}^\dagger = f_{\overline{q} \overline{m}}$ , while the results of Ref. 57 suggest that  $f_{qm}^\dagger = f_{\overline{q} m}$ . We emphasize that these subtle differences between our and original DEOM formulations exist only in the underdamped regime,<sup>71</sup> in which  $\mu_m$ s appear in complex-conjugated pairs. While we expect that the differences would affect dissipaton-resolved quantities, the quantities depending on  $f_{qm}$  only through their sum  $B_q$  [see, e.g., Eq. (16)] do not depend on whether Eq. (12) features  $\delta_{m_1 \overline{m_2}}$  or  $\delta_{m_1 m_2}$ . Most of the previous DEOM-based studies dealt with the (strongly) overdamped regime,<sup>57,58,72,73</sup> in which all  $\mu_m$ s are real ( $\overline{m} = m$ ), so that Eq. (12) reduces to the standard DEOM prescription. The DEOM construction also needs the time-reversal counterpart of Eq. (12), which reads

$$\left\langle f_{q_1 m_1}^{(I)}(0) f_{q_2 m_2}^{(I)}(t) \right\rangle_B = \delta_{m_1 \overline{m_2}} \eta_{q_2 \overline{q_1}}^* e^{-\mu_{m_2} t}. \quad (13)$$

#### D. DEOM-based framework for transport properties

Carrier transport dynamics are encoded in the finite-temperature real-time current-current correlation function<sup>47,48</sup>

$$C_{jj}(t) = \text{Tr} \{ j e^{-i H_{\text{tot}} t} j \rho_{\text{tot}}^{\text{eq}} e^{i H_{\text{tot}} t} \}, \quad (14)$$

where  $\rho_{\text{tot}}^{\text{eq}} = e^{-\beta H_{\text{tot}}} / \text{Tr} \{ e^{-\beta H_{\text{tot}}} \}$ . The current operator  $j = j_e + j_{e-\text{ph}}$  is the sum of the purely electronic (band) current

$$j_e = \sum_k v_k P_k, \quad (15)$$

with  $v_k = \partial_k \varepsilon_k$  and  $P_k = |k\rangle\langle k|$ , and the phonon-assisted current

$$j_{e-\text{ph}} = \sum_q J_q B_q \approx \sum_{kq} \sum_{m=0}^{K-1} M_J(k, q) |k+q\rangle\langle k| f_{qm}, \quad (16)$$

with  $M_J(k, q) = \partial_k M(k, q)$ .<sup>24,25</sup>

Within the DEOM theory, the operator

$$\iota_{\text{tot}}(t) = e^{-i H_{\text{tot}} t} j \rho_{\text{tot}}^{\text{eq}} e^{i H_{\text{tot}} t} \quad (17)$$

is represented by the so-called dissipaton density operators (DDOs)<sup>57,59</sup>

$$\iota_{\mathbf{n}}^{(n)}(t) = \text{Tr}_B \left\{ F_{\mathbf{n}}^{(n)} \iota_{\text{tot}}(t) \right\}. \quad (18)$$

These describe many-dissipaton configurations labeled by the  $(N-1)K$ -dimensional vector  $\mathbf{n} = [n_{qm}]$  of nonnegative integers  $n_{qm}$  such that  $\sum_{qm} n_{qm} = n$ . The bath operator  $F_{\mathbf{n}}^{(n)}$  is the irreducible product of single-dissipaton operators  $f_{qm}$ , which remains invariant under permutations of  $f$  operators.<sup>59</sup> We will need

$$F_{\mathbf{0}}^{(0)} = \mathbb{I}_B, \quad F_{\mathbf{0}_{qm}^+}^{(1)} = f_{qm}. \quad (19)$$

Although we have succeeded in expressing  $F_{\mathbf{n}}^{(n)}$  for  $n \geq 2$  in terms of  $f_{qm}$  in the undamped case,<sup>24</sup> we note that this task is considerably more difficult and still incompletely solved in the dissipative case considered here.<sup>71,74</sup>

The operators  $\iota_{\mathbf{n}}^{(n)}(t)$  satisfy the real-time DEOM (r-DEOM)<sup>57,59</sup>

$$\begin{aligned} \partial_t \iota_{\mathbf{n}}^{(n)}(t) = & -i(H_S^\times - i\mu_{\mathbf{n}}) \iota_{\mathbf{n}}^{(n)}(t) - i \sum_{qm} V_q^\times \iota_{\mathbf{n}_{qm}^+}^{(n+1)}(t) \\ & - i \sum_{qm} n_{qm} \sum_{q'} \left( \eta_{qq'm} V_{q'}^> - \eta_{\overline{q} \overline{q'm}}^* V_{q'}^< \right) \iota_{\mathbf{n}_{qm}^-}^{(n-1)}(t). \end{aligned} \quad (20)$$

In Eq. (20),  $V^\times O = [V, O]$ ,  $V^>O = VO$ ,  $V^<O = OV$ , while  $\mu_{\mathbf{n}} = \sum_{qm} n_{qm} \mu_m$ . At each instant  $t$ , we combine Eqs. (14)–(16) and (17)–(19) to obtain

$$\begin{aligned} C_{jj}(t) = \text{Tr} \{ j \iota_{\text{tot}}(t) \} = & \sum_k v_k \langle k | \iota_{\mathbf{0}}^{(0)}(t) | k \rangle \\ & + \sum_{kqm} M_J(k, q) \langle k | \iota_{\mathbf{0}_{qm}^+}^{(1)}(t) | k+q \rangle. \end{aligned} \quad (21)$$

The r-DEOM in Eq. (20) is propagated starting from the initial condition

$$\iota_{\mathbf{n}}^{(n)}(0) \equiv \iota_{\mathbf{n}}^{(n, \text{eq})} = \text{Tr}_B \left\{ F_{\mathbf{n}}^{(n)} j \rho_{\text{tot}}^{\text{eq}} \right\}, \quad (22)$$

which is to be expressed in terms of the DDOs  $\rho_{\mathbf{n}}^{(n, \text{eq})} = \text{Tr}_B \{ F_{\mathbf{n}}^{(n)} \rho_{\text{tot}}^{\text{eq}} \}$  constituting the DEOM representation of  $\rho_{\text{tot}}^{\text{eq}}$ . The contribution of  $j_e$  to Eq. (22) is

$$\iota_{\mathbf{n}, e}^{(n, \text{eq})} = \text{Tr}_B \left\{ F_{\mathbf{n}}^{(n)} j_e \rho_{\text{tot}}^{\text{eq}} \right\} = \sum_k v_k P_k \rho_{\mathbf{n}}^{(n, \text{eq})}. \quad (23)$$

To evaluate the contribution of  $j_{e-\text{ph}}$  to Eq. (22), we use the generalized Wick's theorem<sup>57,59</sup>

$$\begin{aligned} \text{Tr}_B \left\{ F_{\mathbf{n}}^{(n)} f_{qm} \rho_{\text{tot}}^{\text{eq}} \right\} = & \rho_{\mathbf{n}_{qm}^+}^{(n+1, \text{eq})} + \sum_{q'm'} n_{q'm'} \langle f_{q'm'} f_{qm} \rangle_B^> \rho_{\mathbf{n}_{q'm'}^-}^{(n-1, \text{eq})}, \end{aligned} \quad (24)$$

where [see Eq. (12)]

$$\langle f_{q'm'} f_{qm} \rangle_B^> = \left\langle f_{q'm'}^{(I)}(0_+) f_{qm}^{(I)}(0) \right\rangle_B = \delta_{mm'} \eta_{q'qm'}. \quad (25)$$

Combining Eqs. (16), (24), and (25), we obtain that the contribution of  $j_{e-ph}$  to Eq. (22) reads

$$\begin{aligned} \iota_{n,e-ph}^{(n,eq)} &= \text{Tr}_B \left\{ F_{\mathbf{n}}^{(n)} j_{e-ph} \rho_{\text{tot}}^{\text{eq}} \right\} = \\ &= \sum_{qm} J_q \rho_{\mathbf{n}_{qm}^{+}}^{(n+1,eq)} + \sum_{qm} n_{qm} \sum_{q'} \eta_{qq'm} J_{q'} \rho_{\mathbf{n}_{qm}^{-}}^{(n-1,eq)}. \end{aligned} \quad (26)$$

### E. DEOM representation of the correlated carrier–bath equilibrium

The DEOM representation  $\{\rho_{\mathbf{n}}^{(n,eq)}\}$  of  $\rho_{\text{tot}}^{\text{eq}}$  follows from the imaginary-time DEOM (i-DEOM)<sup>59,75</sup>

$$\begin{aligned} \partial_{\tau} \sigma_{\mathbf{n}}^{(n)}(\tau) &= -(H_S^{\times} - i\mu_{\mathbf{n}}) \sigma_{\mathbf{n}}^{(n)}(\tau) \\ &- \sum_{qm} V_q^> \sigma_{\mathbf{n}_{qm}^{+}}^{(n+1)}(\tau) \\ &- \sum_{qm} n_{qm} \sum_{q'} \eta_{qq'm} V_{q'}^> \sigma_{\mathbf{n}_{qm}^{-}}^{(n-1)}(\tau). \end{aligned} \quad (27)$$

Equation (27) is propagated from  $\tau = 0$  to  $\beta$  with the initial condition

$$\sigma_{\mathbf{n}}^{(n)}(0) = \delta_{n,0} \delta_{\mathbf{n},\mathbf{0}} \frac{e^{-\beta H_S}}{\text{Tr}_S e^{-\beta H_S}}, \quad (28)$$

after which  $\rho_{\mathbf{n}}^{(n,eq)}$  is obtained as

$$\rho_{\mathbf{n}}^{(n,eq)} = \frac{\sigma_{\mathbf{n}}^{(n)}(\beta)}{\text{Tr}_S \sigma_{\mathbf{0}}^{(0)}(\beta)}. \quad (29)$$

### F. Model parameters

We focus on the slow-phonon ( $\omega_0/J = 0.044$ ), high-temperature ( $T/J = 0.175$  or  $T/\omega_0 \approx 4$ ), intermediate-interaction ( $\lambda = 0.336$ ) regime, which is relevant for anisotropic carrier transport in organic molecular crystals.<sup>3,23</sup> The damping parameter  $\gamma_0$  in Eq. (6) can be estimated from combined molecular-dynamics and quantum-chemistry analyses of the vibrational motions that most strongly modulate carrier transport along the maximum-conductivity direction of rubrene<sup>23</sup> and a discotic liquid crystal.<sup>30</sup> Troisi and coworkers<sup>30,31,76</sup> concluded that the carrier–phonon interaction limiting carrier transport in quasi-one-dimensional organic semiconductors can be described by the BO or multimode BO SD. The most prominent mode can be either underdamped [ $\gamma_0/\omega_0 \sim 0.25$  in Fig. 1(b) of Ref. 23] or overdamped ( $\gamma_0/\omega_0 = 1.7$  in Ref. 30). Assuming undamped vibrations, we have recently examined carrier transport for different adiabaticity ratios  $\omega_0/J$ , temperatures, and interactions.<sup>24,25</sup> We

do not expect that the damping of vibrational motions change the trends observed upon varying these parameters. Therefore, here we mostly concentrate on understanding the effect of damping on transport dynamics, which has not been widely explored so far.

### G. Quantities describing carrier transport

The physical quantities that we use to characterize transport dynamics are the time-dependent diffusion constant

$$\mathcal{D}(t) = \frac{1}{2} \frac{d}{dt} \Delta x^2(t) = \int_0^t ds \text{Re } C_{jj}(s), \quad (30)$$

which determines the growth rate of the carrier’s mean-square displacement  $\Delta x^2(t) = \langle [x(t) - x(0)]^2 \rangle$ , and the diffusion exponent

$$\alpha(t) = \frac{2t\mathcal{D}(t)}{\Delta x^2(t)}, \quad (31)$$

which determines the instantaneous power-law growth of  $\Delta x^2(t)$  with time,  $\Delta x^2(t) \propto t^{\alpha(t)}$ . We are mostly interested in how the details of the crossover between short-time ballistic transport, for which  $\alpha(t) \approx 2$ , and long-time diffusive transport, for which  $\alpha(t)$  approaches unity, change upon varying the damping rate  $\gamma_0$ . In experiments, transport dynamics are usually inferred from the dynamical-mobility profile

$$\text{Re } \mu(\omega) = \frac{1 - e^{-\beta\omega}}{2\omega} \int_{-\infty}^{+\infty} dt e^{i\omega t} C_{jj}(t). \quad (32)$$

The dc mobility  $\mu_{\text{dc}} = \text{Re } \mu(\omega = 0)$  is connected to the long-time limit  $\mathcal{D}_{\infty}$  of  $\mathcal{D}(t)$  through the Einstein relation  $\mu_{\text{dc}} = \frac{\mathcal{D}_{\infty}}{T}$ .

### III. TECHNICAL DETAILS

The parameter regime described in Sec. IIF is challenging because the DEOM [Eqs. (27) and (20)] have to be solved on long chains, as implied by the small adiabaticity ratio, and truncated at a moderate maximum depth  $D$  dictated by the combination of high temperature and intermediate interaction. Up to now, the (bosonic) dissipaton algebra has been used to study hybrid system–bath dynamics only in few-level systems (monomers and dimers).<sup>57,58,71–73</sup> Meanwhile, the applications of the (bosonic) DEOM formalism to systems with somewhat larger number of electronic levels focused on purely electronic dynamics.<sup>77–80</sup>

To the best of our knowledge, our study is among the first studies exploiting the (bosonic) dissipaton algebra to compute a finite-temperature real-time correlation function of a mixed system–bath operator in a many-level system. Our computations are made possible by formulating the DEOM in momentum space,<sup>24,62</sup> in which

the DDO  $\iota_{\mathbf{n}}^{(n)}(t)$  in Eq. (20) has only  $N$  (instead of  $N^2$ ) nonzero matrix elements  $\langle k | \iota_{\mathbf{n}}^{(n)}(t) | k + \mathbf{k}_{\mathbf{n}} \rangle$ , and similarly for  $\langle k | \sigma_{\mathbf{n}}^{(n)}(\tau) | k + \mathbf{k}_{\mathbf{n}} \rangle$  in Eq. (27). In Secs. III A–III C, we discuss further technical details needed to gain confidence in our DEOM results.

### A. DEOM closing scheme

Ideally, the r-DEOM in Eq. (20) are to be solved using  $K \rightarrow \infty$  terms in the exponential decomposition in Eq. (11), and considering DDOs up to the maximum depth  $D \rightarrow \infty$ . In practice, both  $K$  and  $D$  are finite, and the convergence with respect to them has to be checked. The convergence can be enhanced by devising appropriate DEOM closing schemes with respect to  $K$  and  $D$ .<sup>57,81,82</sup>

As we focus on high temperatures, at which  $\beta\omega_0 \ll 1$  and  $\beta\gamma_0 \ll 1$ , see Sec. II F, it is justified to set  $K = 2$ , i.e., to retain only the terms originating from the poles of  $\mathcal{J}_{\text{BO}}(\omega)$  in Eq. (11), see Fig. 2(a) and Appendix A. We then employ the Ishizaki–Tanimura closing with respect to  $K$ ,<sup>83,84</sup> augmenting the RHS of Eq. (20) by

$$[\partial_t \iota_{\mathbf{n}}^{(n)}(t)]_K = -\Delta \sum_q V_q^\times V_q^\times \iota_{\mathbf{n}}^{(n)}(t), \quad (33)$$

where<sup>84</sup>

$$\Delta = \sum_{m=K}^{+\infty} \frac{c_m}{\mu_m} = E_0 \left( 4 \frac{T\gamma_0}{\omega_0^2} - i \right) - \sum_{m=0}^{K-1} \frac{c_m}{\mu_m}. \quad (34)$$

It is known that the HEOM/DEOM with BO SD can exhibit long-time numerical instabilities,<sup>61</sup> similar to those observed in models with undamped vibrations,<sup>62,85</sup> which cannot be removed by simply increasing  $D$ . Assuming undamped phonons, for which such instabilities are expected to be the most pronounced, we have shown<sup>24,25,62</sup> that HEOM can be stabilized by introducing the closing term

$$[\partial_t \langle k | \iota_{\mathbf{n}}^{(n)}(t) | k + \mathbf{k}_{\mathbf{n}} \rangle]_D = -\delta_{n,D} \Gamma(k, \mathbf{n}) \langle k | \iota_{\mathbf{n}}^{(n)}(t) | k + \mathbf{k}_{\mathbf{n}} \rangle \quad (35)$$

to the equations at depth  $D$ . In contrast to existing approaches,<sup>57,81,82</sup> which were gauged on few-level systems, the closing term in Eq. (35) does not introduce couplings among either DDOs at depth  $D$  or different matrix elements of a DDO at depth  $D$ . This feature of Eq. (35) guarantees that the computational cost of the closing remains much smaller than that of one step in DEOM propagation. The complex quantity  $\Gamma(k, \mathbf{n})$  depends on the details of the closing, i.e., on the approximations employed to solve the equations at depth  $D + 1$ . Neglecting the couplings to DDOs at depth  $D + 2$ , and using the Markovian and adiabatic approximations yields

$$\Gamma_{\text{MA}}(k, \mathbf{n}) = \frac{1}{2}(\gamma_k + \gamma_{k+\mathbf{k}_{\mathbf{n}}}^*), \quad (36)$$

where

$$\gamma_k = \frac{2}{N} \sum_{qm} \frac{c_m |M(k, q)|^2}{\mu_m + i(\varepsilon_{k+q} - \varepsilon_k)}. \quad (37)$$

Another possibility for closing with respect to  $D$  is the so-called derivative-resum scheme,<sup>57,81,86</sup> which employs

$$\begin{aligned} \Gamma_{\text{DR}}(k, \mathbf{n}) = & \frac{1}{N} \sum_{qm} \frac{c_m |M(k, q)|^2}{\mu_{\mathbf{n}} + \mu_m + i(\varepsilon_{k+q} - \varepsilon_{k+\mathbf{k}_{\mathbf{n}}})} \\ & + \frac{1}{N} \sum_{qm} \frac{c_m^* |M(k + \mathbf{k}_{\mathbf{n}}, q)|^2}{\mu_{\mathbf{n}} + \mu_m + i(\varepsilon_k - \varepsilon_{k+\mathbf{k}_{\mathbf{n}}+q})}. \end{aligned} \quad (38)$$

We have thoroughly presented the procedure to obtain Eqs. (36)–(38) in Appendix D of Ref. 24.

Following the practice common in models without explicit dissipation, in Eq. (35) we retain only real parts of  $\Gamma(k, \mathbf{n})$ , i.e., we neglect the closing-induced renormalization of free-oscillation frequencies of DDOs at the terminal layer. We have checked that the imaginary parts of  $\Gamma(k, \mathbf{n})$  in Eq. (35) very weakly affect the overall transport dynamics, and in particular the long-time transport coefficient  $\mu_{\text{dc}}$ . In undamped models,<sup>24,62</sup>  $\text{Re } \Gamma_{\text{MA}}(k, \mathbf{n})$  and  $\text{Re } \Gamma_{\text{DR}}(k, \mathbf{n})$  are meaningful only in the infinite-chain limit  $N \rightarrow \infty$ , in which these can be evaluated analytically. For  $\gamma_0 \neq 0$ ,  $\text{Re } \Gamma_{\text{MA}}(k, \mathbf{n})$  and  $\text{Re } \Gamma_{\text{DR}}(k, \mathbf{n})$  can be computed for any finite  $N$ , on which they strongly depend. Although analytical expressions for  $\text{Re } \Gamma_{\text{MA}}(k, \mathbf{n})$  and  $\text{Re } \Gamma_{\text{DR}}(k, \mathbf{n})$  in the  $N \rightarrow \infty$  limit are not available for  $\gamma_0 \neq 0$ , we find that their long-chain limits are reached for  $N$  much larger than typical chain lengths  $N \sim 30$  we consider here. In practice, we find that computing Eqs. (37) and (38) on a chain containing  $N_\infty = (10^3 - 10^4)N$  sites provides us with the desired long-chain limits (although  $N_\infty/N$  generally decreases with increasing  $\gamma_0$ ).

In Ref. 25, we have checked that both the Markovian-adiabatic [Eqs. (36) and (37)] and derivative-resum [Eq. (38)] schemes yield virtually identical transport dynamics for  $\gamma_0 = 0$ . Figures 2(b) and 2(c) confirm that the same holds in the overdamped regime  $\gamma_0/\omega_0 = 1.7$ . These also reveal that, for sufficiently strong damping, the so-called time-nonlocal closing,<sup>87</sup> which sets  $\Gamma(k, \mathbf{n}) = 0$  in Eq. (35), also yields stable long-time diffusive dynamics from which low-frequency dynamical mobility can be meaningfully extracted. This stands in sharp contrast to the undamped case, in which computations of long-time transport coefficients crucially require a closing term<sup>25</sup> because these cannot be accessed by extrapolating the results for small nonzero dampings to the zero-damping limit.<sup>68</sup> Although Figs. 2(b) and 2(c) suggest that the closing terms can be omitted if  $\gamma_0$  is sufficiently large, all our results rely on the propagation of the closed DEOM. Using one and the same closing scheme throughout the physically reasonable range for  $\gamma_0$  down to  $\gamma_0 = 0$  enables a consistent and fair assessment of trends in transport dynamics with varying  $\gamma_0$ .

Furthermore, Figs. 2(b) and 2(c) suggest that our DEOM closing enhances not only the convergence with

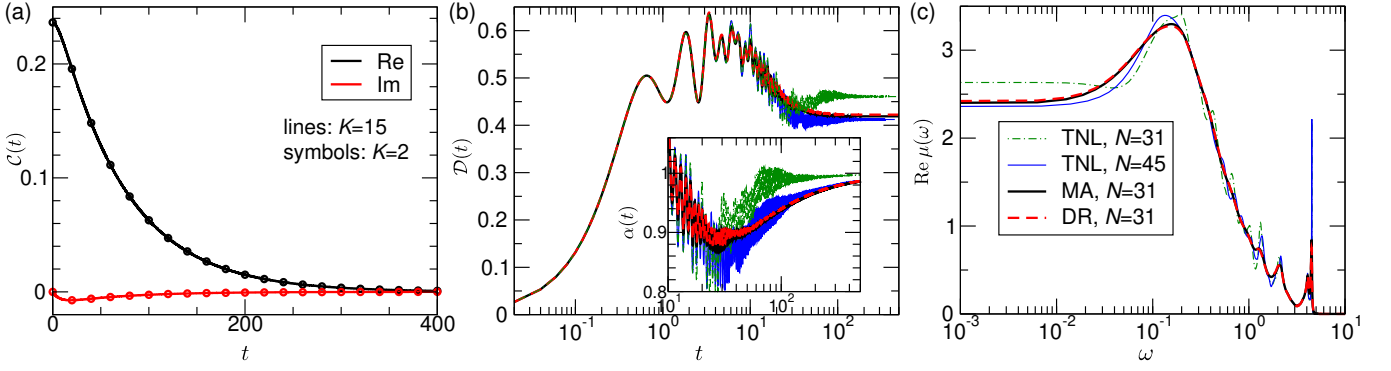


FIG. 2. (a) Real (black) and imaginary (red) parts of the bath correlation function  $\mathcal{C}(t)$  computed using  $K = 2$  (symbols) and  $K = 15$  (lines) terms in the exponential decomposition in Eq. (11). The time-dependent diffusion constant (b) and the dynamical-mobility profile (c) computed using DEOM with  $\Gamma(k, \mathbf{n}) = 0$  in Eq. (35) (label “TNL”, thin lines) and with the Markovian-adiabatic [Eqs. (36) and (37), label “MA”, thick solid line] and derivative-resum [Eq. (38), label “DR”, dashed line] closing terms with respect to  $D$ . The inset of panel (b) compares the diffusion-exponent dynamics computed using the same closing schemes. The model parameters are  $J = 1, \omega_0 = 0.044, \lambda = 0.336, T = 0.175$ , and  $\gamma_0 = 1.7\omega_0$ , while the maximum DEOM depth is  $D = 4$ .

respect to the maximum depth, but also with respect to the chain length. Namely, the DEOM dynamics with  $N = 31$  and Markovian-adiabatic or derivative-resum closing are very similar to those employing a  $\approx 50\%$ -longer chain ( $N = 45$ ) and time-nonlocal closing. In the overdamped regime considered here, the diffusion-constant growth on intermediate timescales and the corresponding dynamical-mobility feature at  $\omega \approx \omega_0$ , see Figs. 2(b) and 2(c) for  $N = 31$ , reflect finite-size effects. Meanwhile, analogous features for weak damping are not artifacts due to insufficient chain length,<sup>25</sup> as discussed in greater detail in Sec. III C.

Finally, we prefer the Markovian-adiabatic [Eqs. (36) and (37)] to the derivative-resum [Eq. (38)] scheme because of its more favorable computational requirements. Namely, the Markovian-adiabatic scheme needs only  $N$  quantities  $\gamma_k$  computed on an  $N_\infty$ -site chain, while the derivative-resum scheme needs a much larger number of quantities  $\Gamma_{\text{DR}}(k, \mathbf{n})$ ,  $N$  quantities for each DDO at depth  $D$ . Although all these quantities can be computed only once, before the r-DEOM propagation, our derivative-resum scheme requires much more computational time and computer memory to compute and store the closing terms than the Markovian-adiabatic scheme. It is for this reason that we employ the Markovian-adiabatic scheme in the following.

## B. Thermodynamic quantities

The i-DEOM in Eq. (27) is constructed by the analytical continuation of the dissipaton algebra,<sup>75</sup> which amounts to setting  $t = -i\tau$  ( $0 \leq \tau \leq \beta$ ) in Eq. (11). The first equality in Eq. (11) shows that the function  $\tilde{\mathcal{C}}(\tau) = \mathcal{C}(-i\tau)$  is purely real and symmetric around  $\beta/2$ , i.e.,  $\tilde{\mathcal{C}}(\beta - \tau) = \tilde{\mathcal{C}}(\tau)$ . However, the exponential decomposition in Eq. (11) does not satisfy these two requirements

for finite values of  $K$ . For  $K = 2$ , on which we focus here, the exponential decomposition satisfies

$$\sum_{m=0}^1 c_m e^{i\mu_m(\beta-\tau)} = \left( \sum_{m=0}^1 c_m e^{i\mu_m\tau} \right)^* \approx \sum_{m=0}^1 c_m e^{i\mu_m\tau}. \quad (39)$$

The first equality can be checked using the results of Appendix A, while the approximate equality is appropriate for the slow bath and at high temperatures considered here, when both  $\mathcal{C}(t)$  [see Fig. 2(a)] and  $\tilde{\mathcal{C}}(\tau)$  are almost purely real (the bath is in a good approximation classical). We note that the exponential decomposition of  $\tilde{\mathcal{C}}(\tau)$  for undamped vibrations<sup>24,25,62,88</sup> satisfies the reality and symmetry requirements exactly.

The fact that the symmetries of  $\tilde{\mathcal{C}}(\tau)$  are obeyed only approximately, as well as the existence of various connections between single-carrier levels induced by the hierarchical couplings between DDOs, may suggest that the solution of the i-DEOM in Eq. (27) does not provide a faithful representation of the correlated carrier-bath equilibrium.<sup>75</sup> Indeed, while the reduced carrier populations  $\langle k | \rho_0^{(0,\text{eq})} | k \rangle$  are purely real for  $\gamma_0 = 0$ ,<sup>24,25,62,88</sup> we find that the solution of the i-DEOM for  $\gamma_0 \neq 0$  yields complex populations and complex carrier’s kinetic energy

$$\langle H_S \rangle = \sum_k \varepsilon_k \langle k | \rho_0^{(0,\text{eq})} | k \rangle. \quad (40)$$

Also, the carrier-bath interaction energy

$$\langle H_{S-B} \rangle \approx \sum_{kq} M(k, q) \sum_{m=0}^{K-1} \langle k | \rho_{0_q^+}^{(1,\text{eq})} | k + q \rangle \quad (41)$$

has a nonzero imaginary part, in contrast to the undamped case.<sup>24,25</sup> Although Fig. 3(a) shows that both



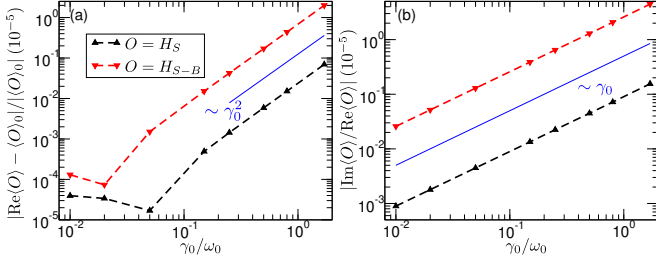


FIG. 3. (a) Magnitude of the relative deviation of the real part of the carrier's kinetic energy [Eq. (40), up-triangles connected by a dashed line] and the carrier-bath interaction energy [Eq. (41), down-triangles connected by a dashed line] from the corresponding values at zero damping (denoted by  $\langle O \rangle_0$ ) as a function of the damping parameter. (b) The magnitude of the ratio of the imaginary to the real part of the quantities considered in panel (a) as a function of the damping parameter. In both panels, the quantities on vertical axes are given in units of  $10^{-5}$ , while solid lines show the appropriate power-law scalings. The propagation of the i-DEOM [Eq. (27)] over the interval  $[0, \beta]$  used 1000 imaginary-time steps.

$\text{Re} \langle H_S \rangle$  and  $\text{Re} \langle H_{S-B} \rangle$  grow quadratically with  $\gamma_0$  (for sufficiently large  $\gamma_0$ ), they are virtually equal to the corresponding values in the undamped case for physically plausible values of  $\gamma_0$ . Figure 3(b) shows that  $\text{Im} \langle H_S \rangle$  and  $\text{Im} \langle H_{S-B} \rangle$  grow linearly with  $\gamma_0$ , but remain quite small with respect to the corresponding real parts throughout the physically relevant range  $\gamma_0/\omega_0 \lesssim 2$ . Therefore, the real parts of Eqs. (40) and (41) obtained using the i-DEOM remain representative of the kinetic and interaction energies, respectively.

The above-described deficiencies of the DEOM representation of  $\rho_{\text{tot}}^{\text{eq}}$  following from the i-DEOM can in principle be avoided by propagating the r-DEOM up to very long real times or computing its steady state directly.<sup>89</sup> However, for the parameters considered here, we find that these r-DEOM-based strategies, tried and tested on systems immersed in overdamped baths, perform poorly.

### C. Finite-depth and finite-chain effects for weak damping

Here, we discuss the maximum DEOM depth  $D$  and chain length  $N$  needed to obtain transport properties representative of the large- $D$  and large- $N$  limit.

In our recent study,<sup>25</sup> which uses  $\gamma_0 = 0$ , we have found that  $N = 31$  is sufficient to keep finite-chain effects under control, while  $D = 4$  is the largest depth for which the hierarchy closing scheme is effective. Generally speaking, introducing friction renders finite-size and non-Markovian effects less pronounced, and we expect that the values  $N = 31$  and  $D = 4$  remain representative of the large- $N$  and large- $D$  limit also for  $\gamma_0 \neq 0$ . However, in Ref. 25, we also concluded that larger values of  $D$ , required to fully converge  $\langle H_S + H_{S-B} \rangle$  with respect to  $D$ , may be needed to firmly numerically confirm the

optical sum rule

$$\int_0^{+\infty} d\omega \text{Re} \mu(\omega) = -\frac{\pi}{2} \text{Re} \langle H_S + H_{S-B} \rangle. \quad (42)$$

Since a small but nonzero friction generally stabilizes the dynamics, we are now in a position to increase  $D$  beyond 4 (at the expense of decreasing  $N$ ), which we do in Figs. 4(a)–4(c) for  $\gamma_0/\omega_0 = 0.05$ .

Fixing  $N = 21$  or 31, we observe that transport properties computed for  $D = 4, 5, 6$  or  $D = 4, 5$  are qualitatively similar, though there are some quantitative differences. Namely, the growth of  $\mathcal{D}(t)$  beyond  $\mathcal{D}(t_{\min})$  [Fig. 4(a)], where  $t_{\min} \approx 1/\omega_0$ , the overshoot of  $\alpha(t)$  above unity on intermediate timescales [Fig. 4(b)], and the dynamical-mobility enhancement below  $\omega_0$  [Fig. 4(c)] are more pronounced with increasing  $D$ . Meanwhile, increasing  $D$  does not change either the position or shape of the displaced Drude peak [Fig. 4(c)], while quantitative changes in transport properties upon increasing  $D$  are of the order of 10%.<sup>25</sup> As DEOM computations for  $D = 5$  (let alone  $D = 6$ ) require significantly more computational resources than those employing  $D = 4$ , we opt for  $D = 4$  as a good compromise between computational effort and accuracy. The relative accuracy with which the OSR [Eq. (42)] is satisfied is  $\sim 10^{-4}$  for all depths considered.

Fixing  $D = 4$  ( $D = 5$ ), we find that  $\mathcal{D}(t)$ ,  $\alpha(t)$ , and  $\text{Re} \mu(\omega)$  for  $N = 21, 31$ , and 45 ( $N = 21$  and 31) are qualitatively and to a large extent quantitatively similar. Finite-chain effects on the dynamics of  $\mathcal{D}$  and  $\alpha$  come into play for  $t \gtrsim \pi/\omega_0$ , see the insets of Figs. 4(a) and 4(b). We observe that increasing  $N$  renders the increase in  $\mathcal{D}(t)$  for  $t \gtrsim t_{\min}$ , the overshoot of  $\alpha(t)$  above unity, and the dynamical-mobility enhancement below  $\omega_0$  somewhat less pronounced. One might thus object to the relevance of these features in the long-chain limit. To refute such an objection, we note that the very same features have been observed in fully quantum<sup>90</sup> or quantum-classical<sup>21,91–93</sup> approaches to carrier transport in models with local<sup>90,91</sup> or nonlocal<sup>21,92,93</sup> interaction of a carrier with undamped<sup>21,90–93</sup> or moderately damped<sup>21</sup> vibrations. In particular, the quantum-classical study in Ref. 21 considered the same adiabaticity  $\omega_0/J$  ratio as here, and observed the same long-time (low-frequency) features in  $\mathcal{D}(t)$  [ $\text{Re} \mu(\omega)$ ] on chains with hundreds of sites. By assuming classical vibrational dynamics, which is appropriate for small  $\omega_0/J$  and at the high temperature considered here, quantum-classical methods manage to reach what would be the  $D \rightarrow \infty$  limit in the DEOM language. Keeping in mind that increasing  $D$  beyond 4 renders the long-time (low-frequency) features more pronounced, their existence for small  $\gamma_0$  can be considered as firmly established.

The above observations strengthen the conclusions we reached in the dissipationless case,<sup>25</sup> firmly establishing the transient nature of the super-to-subdiffusive crossover and the low-frequency enhancement in the carrier's optical response in the case of weakly damped vibrations moderately coupled to the carrier.



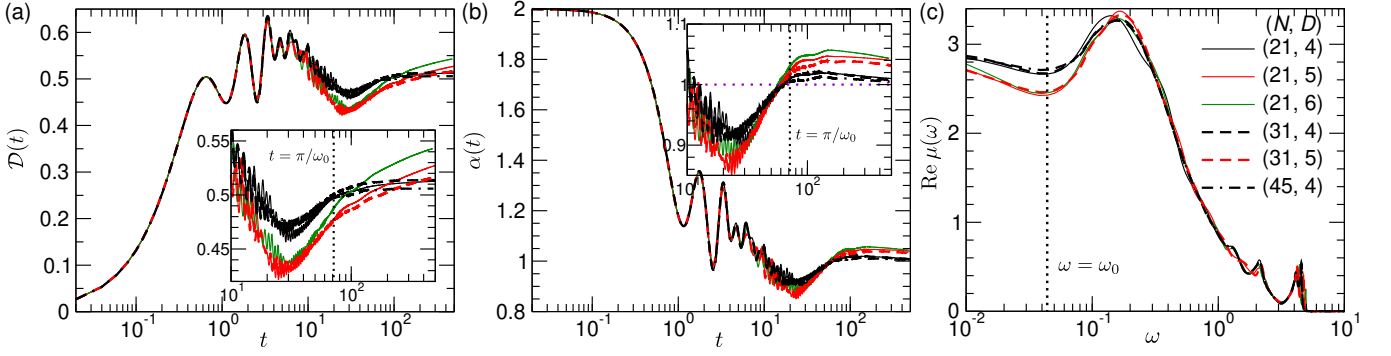


FIG. 4. Dynamics of (a) the diffusion constant  $\mathcal{D}$  and (b) the diffusion exponent  $\alpha$  for different values of the chain length  $N$  and maximum hierarchy depth  $D$ . (c) The dynamical-mobility profile  $\text{Re } \mu(\omega)$  for different values of  $N$  and  $D$ . The insets in (a) and (b) zoom in the dynamics of  $\mathcal{D}$  and  $\alpha$ , respectively, on intermediate-to-long timescales. The model parameters are  $J = 1$ ,  $\omega_0 = 0.044$ ,  $\lambda = 0.336$ ,  $T = 0.175$ , and  $\gamma_0/\omega_0 = 0.05$ . Note the logarithmic scale on horizontal axes.

## IV. RESULTS

### A. Influence of damping on transport dynamics

In Figs. 5(a)–5(c), we monitor the changes to transport quantities brought about by the damping of vibrational motions.

Figures 5(a) and 5(b) reveal that a realistically strong damping of vibrational motions starts to influence carrier dynamics on intermediate timescales (for  $t \gtrsim t_{\min} \approx 1/\omega_0$ ). Therefore, realistically strong damping does not change the position and weakly affects the shape of the displaced Drude peak, see Fig. 5(c), which reflects short-time carrier dynamics in the field of effectively frozen vibrations.<sup>3,15,91</sup> The timescale  $\tau_{\text{diff}}$  on which the diffusive carrier dynamics is established can be estimated as the characteristic timescale for the decay of the current autocorrelation function, which can be defined as [see also Eq. (47)]

$$\tau_{\text{diff}} = \int_0^{+\infty} dt \frac{\text{Re } C_{jj}(t)}{\text{Re } C_{jj}(0)} = \frac{\mathcal{D}_{\infty}}{\langle j^2 \rangle}. \quad (43)$$

Equation (43) involves the long-time diffusion constant, which somewhat decreases with damping,<sup>68</sup> see the inset of Fig. 5(a), and the thermodynamic quantity  $\langle j^2 \rangle$ , which is expected to be virtually independent of the damping, see Sec. III B. While the approach towards diffusive transport becomes somewhat more rapid with increasing damping, the order of magnitude of  $\tau_{\text{diff}}$  remains constant for realistic values of  $\gamma_0$ .

Increasing  $\gamma_0$  renders the intermediate-time growth of  $\mathcal{D}(t)$  less pronounced until it is fully suppressed for  $\gamma_0/\omega_0 \gtrsim 0.5$ , see the inset of Fig. 5(a). Interestingly, the magnitude of the growth, quantified by  $\mathcal{D}_{\infty} - \mathcal{D}(t_{\min})$ , determines whether the super-to-subdiffusive crossover is transient or permanent, see Fig. 5(b), as well as the low-frequency features of the dynamical mobility, see Fig. 5(c). For  $\gamma_0/\omega_0 = 0.05$  and  $0.15$ ,  $\mathcal{D}_{\infty} - \mathcal{D}(t_{\min})$  is sufficiently large so that the diffusive transport sets in

from the superdiffusive side, giving rise to the enhancement in the dynamical mobility below the vibrational frequency. Although  $\mathcal{D}_{\infty} - \mathcal{D}(t_{\min})$  remains positive for  $\gamma_0/\omega_0 = 0.25$ , we find that its magnitude is such that the diffusive transport is approached from the subdiffusive side, while there is almost no low-frequency enhancement in the dynamical mobility, see also Fig. 6(b).

### B. Success of the transient localization phenomenology

Notably, the approach to diffusive dynamics from the subdiffusive side and the absence of dynamical-mobility enhancements below phonon frequency, which persist for  $\gamma_0/\omega_0 \gtrsim 0.25$ , coincide with the predictions of the TLS.<sup>3,15</sup> The TLS starts from the frozen-phonon limit, as appropriate on short timescales  $t \ll \omega_0^{-1}$ , and assumes that the long-time carrier diffusion, absent in the frozen-phonon limit,<sup>94</sup> is reached through effective carrier-phonon dynamics. In the relaxation-time approximation,<sup>3,15</sup> this amounts to

$$C_{jj}^{\text{TLS}}(t) = C_{jj}^{\text{dis}}(t) e^{-|t|/\tau_d}, \quad (44)$$

where  $C_{jj}^{\text{dis}}(t)$  is the current autocorrelation function of the corresponding model with static disorder in nearest-neighbor hopping amplitudes. Rewriting  $H_{S-B}$  in Eq. (1) in real space,

$$H_{S-B} = \sum_n (|n\rangle\langle n+1| + |n+1\rangle\langle n|) \times \sum_{\xi} g_{\xi} (b_{n\xi}^{\dagger} + b_{n\xi} - b_{n+1,\xi}^{\dagger} - b_{n+1,\xi}), \quad (45)$$

the statically disordered model is constructed by formally replacing the phonon operator

$$\sum_{\xi} g_{\xi} (b_{n\xi}^{\dagger} + b_{n\xi} - b_{n+1,\xi}^{\dagger} - b_{n+1,\xi})$$

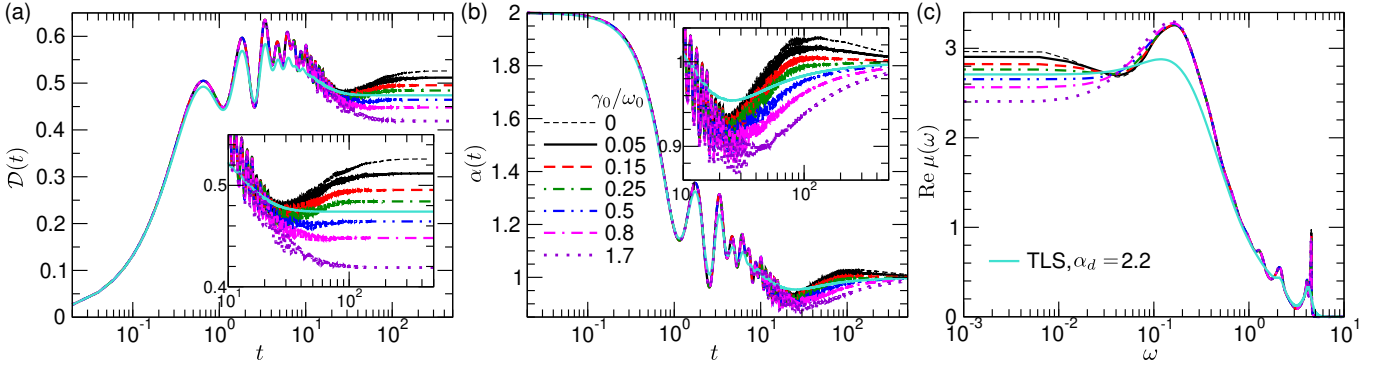


FIG. 5. Dynamics of (a) the diffusion constant  $D$  and (b) the diffusion exponent  $\alpha$  for different values of the friction coefficient  $\gamma_0$ . (c) The dynamical-mobility profile  $\text{Re } \mu(\omega)$  for different values of  $\gamma_0$ . The TLS predictions employ  $\alpha_d = 2.2$ . The insets in (a) and (b) display the dynamics of  $D$  and  $\alpha$ , respectively, on intermediate-to-long timescales. The model parameters are  $J = 1$ ,  $\omega_0 = 0.044$ ,  $\lambda = 0.336$ ,  $T = 0.175$ . DEOM computations are performed for  $N = 31$ ,  $D = 4$ . Note the logarithmic scale on horizontal axes.

by the Gaussian random variable  $X_{n,n+1}$  of zero mean and variance

$$\sigma^2 = \sum_{\xi} 2 \frac{2g_{\xi}^2}{\beta\omega_{\xi}} = 2\lambda JT. \quad (46)$$

We have used that the expectation value of the operator  $g_{\xi}(b_{n\xi}^{\dagger} + b_{n\xi})$  is distributed according to the Gaussian distribution of zero mean and variance  $g_{\xi}^2 \coth(\beta\omega_{\xi}/2) \approx 2g_{\xi}^2/(\beta\omega_{\xi})$ .<sup>91</sup> The approximate equality holds for  $\beta\omega_{\xi} \ll 1$ , as appropriate in the high-temperature slow-phonon regime (see Sec. II F) and on short timescales we consider. As the operators  $g_{\xi}(b_{n\xi}^{\dagger} + b_{n\xi})$  commute for different values of  $n$  or  $\xi$ , the expectation value of their sum over  $\xi$  is distributed in the same way as the sum of mutually independent Gaussian variables, each of which has zero mean and variance  $2g_{\xi}^2/(\beta\omega_{\xi})$ , thus justifying Eq. (46). Equation (46) additionally reveals that the reference statically disordered model does not depend on the details of the carrier-phonon SD or phonon dynamics [Eq. (11)], but only on the overall interaction strength quantified by the dimensionless parameter  $\lambda$ . This once again reflects the fact that the statically disordered model is appropriate only on short timescales.

The timescale  $\tau_d$  in Eq. (44), after which phonon dynamics cannot be neglected, is assumed as  $\tau_d^{-1} = \alpha_d \omega_0$ ,<sup>3,15</sup> where the free parameter  $\alpha_d \sim 1$  can be fine-tuned to best reproduce some reference (experimental or numerical) result for  $\mu_{\text{dc}}$  without qualitatively affecting TLS predictions for transport dynamics. In Figs. 5(a)–5(c), we show the TLS result using  $\alpha_d = 2.2$ . This value was suggested by comparing TLS and reference numerically exact results in Refs. 95 and 96, which considered undamped vibrations. Here, this standard choice for  $\alpha_d$  gives  $\mu_{\text{dc}}^{\text{TLS}}$  that differs by at most 20% from the corresponding DEOM results for physically reasonable damping strengths, see the inset of Fig. 5(a). Importantly, both the TLS with  $\alpha_d = 2.2$  and DEOM with physically relevant values of  $\gamma_0$  yield  $\mu_{\text{dc}}$  that falls into the exper-

imental range  $\mu_{\text{dc}}^{\text{exp}} \sim (10 - 20) \text{ cm}^2/(\text{Vs})$  for the room-temperature dc mobility in rubrene<sup>97–99</sup> [our DEOM mobility is measured in units of  $e_0 a_l^2/\hbar$ , corresponding to  $7.9 \text{ cm}^2/(\text{Vs})$  for  $a_l = 7.2 \text{ \AA}$ , see, e.g., Ref. 23].

Therefore, Figs. 5(a)–5(c) strongly suggest that the damping in intermolecular motions, which is inevitably present in a realistic material,<sup>23,30–32,76</sup> is behind the success of the transient-localization phenomenology (and the related Drude-Anderson framework) in explaining the experimental carriers' optical response. Notably, the damping does not have to be excessively strong in order for DEOM results to comply with the transient-localization phenomenology. Figures 5(a)–5(c) reveal that this happens already for  $\gamma_0/\omega_0 \gtrsim 0.25$ , which belongs to the underdamped regime characterized by a pronounced peak in the SD, see Fig. 1. We thus propose that the optical-absorption enhancements below the vibrational frequency reported in model-Hamiltonian studies assuming undamped vibrations<sup>21,25,90–93</sup> are to be regarded as artifacts of undamped vibrations.

### C. A closer look into the TLS phenomenological timescale

Here, we connect the parameter  $\tau_d$  in Eq. (44) with the characteristic timescale  $\tau_c$  of phonon-induced fluctuations of the transfer integral. In the dissipative model studied here,  $\tau_c$  can be estimated as<sup>60</sup>

$$\tau_c = \int_0^{+\infty} dt \frac{\Psi(t)}{\Psi(0)} = 2 \frac{\gamma_0}{\omega_0^2}, \quad (47)$$

where  $\Psi(t) = -2 \int_t^{+\infty} ds \text{Im } \mathcal{C}(s)$  is the so-called relaxation function.<sup>48,60</sup> For  $\gamma_0/\omega_0 \gtrsim 0.25$ , for which  $\alpha(t)$  and  $\text{Re } \mu(\omega)$  display TL phenomenology, we extract  $\alpha_d = (\omega_0 \tau_d)^{-1}$  by requiring that the dc mobility within the TLS is identical to the corresponding DEOM result. Figure 6(a) shows that thus extracted  $\alpha_d$  is correlated with  $\tau_c$ , see the powerlaw fit (solid line) whose parameters are

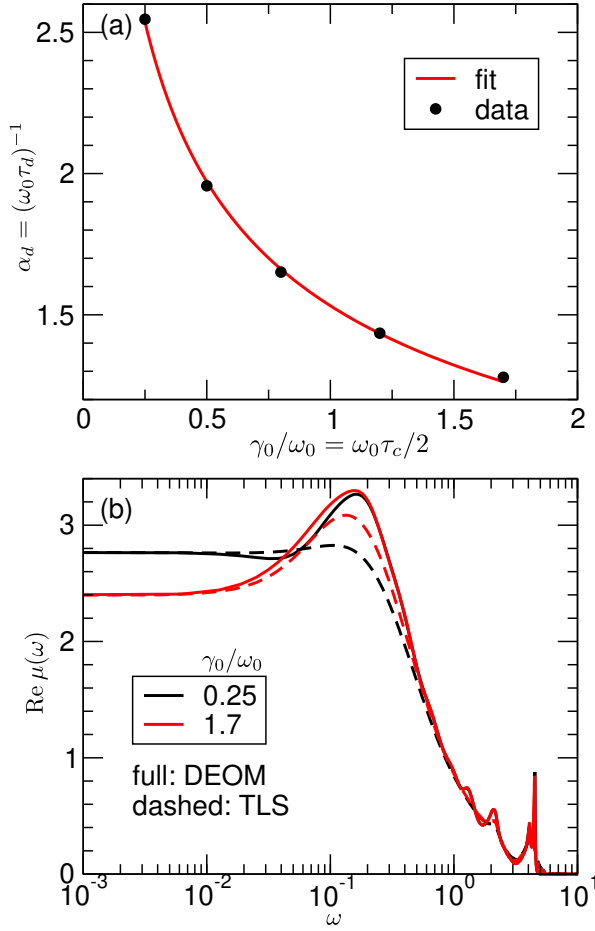


FIG. 6. (a) TLS parameter  $\alpha_d = (\omega_0 \tau_d)^{-1}$  [Eq. (44)], chosen so that  $\mu_{dc}^{\text{TLS}} = \mu_{dc}^{\text{DEOM}}$ , as a function of  $\gamma_0/\omega_0 = \omega_0 \tau_c/2$  [Eq. (47)]. The best power-law fit  $\alpha_d = a_0(\gamma_0/\omega_0)^{-a_1}$ , with  $a_0 = 1.53$  and  $a_1 = 0.364$ , of the data (dots) is shown as a solid line. (b) The comparison of DEOM (solid lines) and TLS [with  $\alpha_d$  chosen as in panel (a), dashed lines] dynamical-mobility profiles for  $\gamma_0/\omega_0 = 0.25$  (black) and 1.7 (red).

summarized in the caption. Interestingly,  $\tau_d = (\alpha_d \omega_0)^{-1}$  somewhat increases with the damping, without changing its order of magnitude, contrary to the timescale  $\tau_{\text{diff}}$  on which carrier dynamics become diffusive, see Sec. IV A. [Since we choose  $\tau_d$  so that  $\mu_{dc}^{\text{TLS}} = \mu_{dc}^{\text{DEOM}}$ , and since  $C_{jj}(0)$  is identical within TLS and DEOM, Eq. (43) shows that  $\tau_{\text{diff}}$  is also identical within TLS and DEOM.] Such a trend in  $\tau_d$  with increasing  $\gamma_0$  is compatible with the dc mobility decreasing with  $\gamma_0$ , see Figs. 5(a) and 5(c). Namely, as vibrations become more damped, the model becomes increasingly similar to that with only static disorder,<sup>31</sup> and this reference point of the TLS is gradually approached as  $\tau_d$  is increased, see Eq. (44). This is discussed in more detail in Appendix B.

If we choose  $\alpha_d$  so that the TLS perfectly reproduces DEOM mobility, the overall agreement between TLS and DEOM dynamical-mobility profiles improves with increasing  $\gamma_0$ , see Fig. 6(b). At smaller damping strengths,

the requirement  $\mu_{dc}^{\text{TLS}} = \mu_{dc}^{\text{DEOM}}$  makes the TLS almost completely miss the DDP, see the curves for  $\gamma_0/\omega_0 = 0.25$  in Fig. 6(b). Although a more accurate TLS approximation to the numerically exact DDP would underestimate the dc mobility,  $\mu_{dc}^{\text{TLS}}$  would still be of the same order of magnitude as  $\mu_{dc}^{\text{DEOM}}$ . Meanwhile, at larger damping strengths, the TLS can reproduce reasonably well both  $\mu_{dc}$  and the position, intensity, and shape of the DDP, see the curves for  $\gamma_0/\omega_0 = 1.7$  in Fig. 6(b). For even stronger dampings, we expect that the dependence of  $\tau_d$  on  $\gamma_0$  is different from that in Fig. 6(a). In Appendix B, we argue that  $\tau_d$  should depend linearly on  $\gamma_0$  in the strong-damping limit.

#### D. Transport dynamics for the Drude-Lorentz spectral density

For the DL SD [Eq. (9)], the short-time behavior of the free-bath correlation function [Eq. (11)] is unphysical because its imaginary part<sup>33,34</sup>

$$\text{Im } \mathcal{C}_{\text{DL}}(t) = -E_0 \gamma_{\text{DL}} e^{-\gamma_{\text{DL}} t} \quad (48)$$

does not vanish at  $t = 0$  as it should.<sup>60,100</sup> The fact that  $\text{Im } \mathcal{C}_{\text{DL}}(0) \neq 0$  is connected to the long tail of  $\mathcal{J}_{\text{DL}}(\omega)$  in the high-frequency region, and underscores the coarse-grained nature of the short-time dynamics.<sup>60,100</sup> This drawback of the DL SD is not expected to appreciably affect carrier transport dynamics inferred from  $C_{jj}(t)$  in Holstein-like models,<sup>41,45,46,49,51</sup> in which there is no phonon-assisted current. Meanwhile, in models with non-local carrier-phonon interaction, the coarse-grained nature is reflected in the unphysical initial condition  $\langle j_{e-\text{ph}}^2 \rangle$  for the phonon-assisted contribution  $\langle j_{e-\text{ph}}(t) j_{e-\text{ph}}(0) \rangle$  to  $C_{jj}(t)$ , which we discuss in more detail in Appendix C. This issue is avoided through the procedure by Ishizaki,<sup>60</sup> which also helps us keep the number of exponentially decaying terms in Eq. (11) low.

Considering the DL SD, the model parameters are usually chosen as in Ref. 40, so that  $J = 300 \text{ cm}^{-1}$ ,  $2E_0 = 323 \text{ cm}^{-1}$ , and  $\gamma_{\text{DL}} = 41 \text{ cm}^{-1}$ . However, the models considered in Refs. 40 and 44 somewhat differ from the model we consider. Namely, the nearest-neighbor hopping amplitude in Ref. 40 (Ref. 44) is modulated by the displacement of the oscillator on the left end of a bond (the center of a bond), so that the dimensionless interaction constant is  $\lambda = \frac{E_0}{J}$ . This is in contrast to our definition  $\lambda = \frac{2E_0}{J}$ , which reflects the fact that the hopping amplitude is modulated by the difference of the displacements on two ends of a bond. Importantly,  $\lambda \approx 0.5$  in Refs. 40 and 44, which belongs to the intermediate-interaction regime relevant for organic molecular crystals.<sup>5</sup>

Figures 7(a) and 7(b) present DEOM results for Ishizaki's BO approximation to the DL SD<sup>60</sup> assuming that  $J = 300 \text{ cm}^{-1}$ ,  $E_0 = 75 \text{ cm}^{-1}$  ( $\lambda = 0.5$ ),  $\gamma_0 = 2\gamma_{\text{DL}} = 80 \text{ cm}^{-1}$  ( $\gamma_0/J = 4/15$ ),  $\epsilon = \gamma_0/4 = 20 \text{ cm}^{-1}$

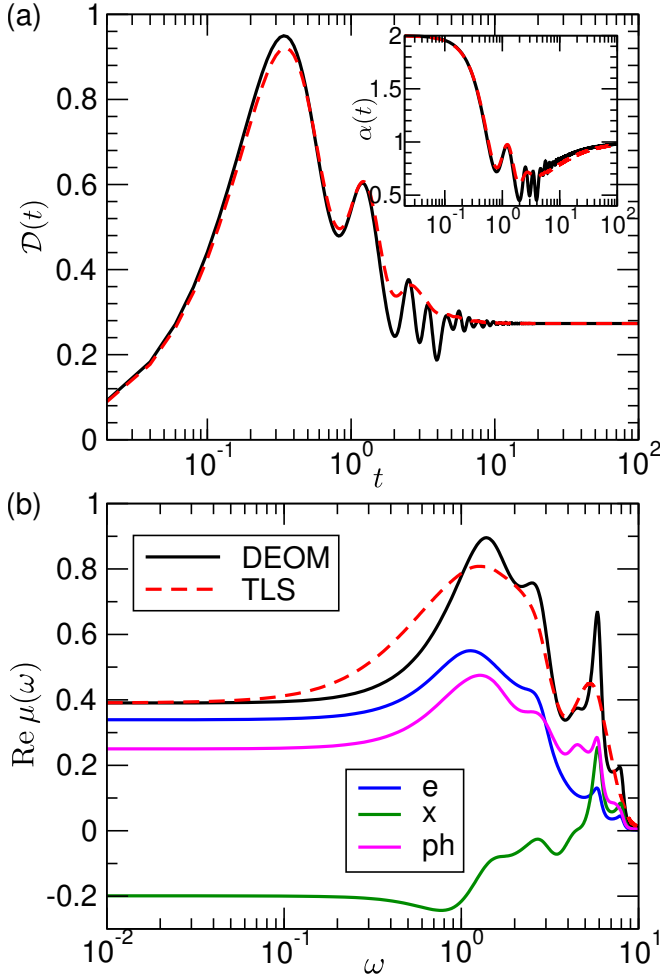


FIG. 7. Time-dependent diffusion constant  $\mathcal{D}(t)$  (a) and the dynamical-mobility profile  $\text{Re } \mu(\omega)$  (b) computed assuming the DL SD and using the DEOM (solid line) and TLS (dashed line). The TLS parameter  $\alpha_d = (\gamma_{\text{DL}}\tau_d)^{-1} = 1.66$  is chosen so that  $\mu_{\text{dc}}^{\text{DEOM}} = \mu_{\text{dc}}^{\text{TLS}}$ . The inset of panel (a) displays the dynamics of the diffusion exponent  $\alpha$ . Panel (b) also shows the purely electronic (label "e"), phonon-assisted (label "ph"), and cross (label "x") contributions to  $\text{Re } \mu(\omega)$ . The model parameters are  $J = 1$ ,  $\gamma_{\text{DL}} = 2/15$ ,  $\lambda = 0.5$ ,  $T = 0.7$ .

( $\gamma_0/\omega_0 = 4/\sqrt{17}$ ), at room temperature  $T = 210 \text{ cm}^{-1}$  ( $T/J = 0.7$ ). DEOM computations are performed using  $N = 11$ ,  $D = 8$ , and  $K = 2$ . We have checked that increasing  $D$  from 8 to 9 or retaining more than two terms in the exponential decomposition of Eq. (11) ( $K = 3$  or 4 with  $N = 7$ ) introduces only minor quantitative changes to the DEOM result for  $N = 11$ ,  $D = 8$ ,  $K = 2$ . We have also checked that employing a smaller value of  $\epsilon = \gamma_0/20$  does not change (either qualitatively or quantitatively) the results using  $\epsilon = \gamma_0/4$ .

The DEOM results in Figs. 7(a) and 7(b) can be well reproduced by the TL phenomenology using the phenomenological timescale  $\tau_d^{-1} = \alpha_d \gamma_{\text{DL}}$  with  $\alpha_d \sim 1$ . Requiring that  $\mu_{\text{dc}}^{\text{DEOM}} = \mu_{\text{dc}}^{\text{TLS}}$ , we obtain  $\alpha_d = 1.66$ . The good performance of the exponential ansatz in Eq. (44)

for the DL SD is connected to the corresponding bath correlation function containing only exponentially decaying terms, the most dominant one being proportional to  $e^{-\gamma_{\text{DL}}t}$ .

Finally, for the usual choice of model parameters of the DL SD at room temperature,<sup>40,44</sup> the phonon-assisted contribution to  $\mu_{\text{dc}}$  [obtained by considering only  $\langle j_{\text{e-ph}}(t)j_{\text{e-ph}}(0) \rangle$  in Eq. (32)] is comparable to the purely electronic contribution to  $\mu_{\text{dc}}$  [obtained by considering only  $\langle j_{\text{e}}(t)j_{\text{e}}(0) \rangle$  in Eq. (32)], see Fig. 7(b). This is different from the situation for model parameters we use with BO SD at room temperature, for which the phonon-assisted contribution is much smaller than the purely electronic contribution to  $\mu_{\text{dc}}$ <sup>25</sup> irrespective of the damping analyzed. The reason behind this difference lies in the different values of the transfer integral considered in the two models. Namely, the authors of Ref. 40 suggest that the Holstein-type interaction with high-frequency intramolecular vibrations leads to an effective reduction of the hopping amplitude from its bare value  $J \approx 1150 \text{ cm}^{-1}$  (see, e.g., 23) to the dressed value  $J \approx 300 \text{ cm}^{-1}$ . Keeping this in mind, and remembering that the value of  $\lambda$  used with the DL SD (0.5) is somewhat larger than that used with the BO SD (0.336), it is not surprising that the dc mobility in the parameter regime discussed in Refs. 40 and 44 is almost an order of magnitude smaller than in the regime analyzed in Fig. 5, compare Fig. 7(b) to Fig. 5(c).

## V. SUMMARY AND OUTLOOK

In this study, we have considered an underexplored aspect of carrier transport in molecular semiconductors, namely, the influence of the damping of vibrational motions on transport dynamics. In contrast to many previous studies, which inferred transport properties from carrier dynamics starting from the factorized initial condition, our considerations are based on the numerically exact quantum dynamics of the current autocorrelation function of a one-dimensional dissipative model with non-local carrier-vibrational interaction. We use the DEOM representation of quantum dynamics, whose dissipaton algebra is essential to correctly treat the phonon-assisted current.

Whenever weakly damped (or undamped) vibrational dynamics are taken seriously, either numerically exactly or approximately, the diffusive carrier dynamics in the physically relevant high-temperature intermediate-interaction regime sets in from the superdiffusive side, giving rise to enhancements in the dynamical mobility below the vibrational frequency. Considering damping strengths characteristic of realistic materials, we find that the diffusive transport is approached from the subdiffusive side, and that the dynamical mobility exhibits no low-frequency upturns. Notably, this is in qualitative agreement with the majority of experimental results and the widely used transient localization scenario. Our find-

ings explain the success of the exponentially decaying ansatz underlying the TLS in rationalizing experimental data. We suggest that low-frequency enhancements in the dynamical-mobility profiles in minimal models reflect the widely used assumption of undamped vibrations.

On the theoretical side, our study represents one of the pioneering applications of the DEOM formalism to computations of finite-temperature real-time correlation functions in dissipative electron–phonon models with more than few electronic levels and nonlocal electron–phonon interaction. We have also discussed the pitfalls of the widely used Drude–Lorentz bath model, which become apparent when considering mixed system–bath quantities, and how to avoid them. Thanks to the physically justified high-temperature assumption, our momentum-space formulation, and an appropriate DEOM closing with respect to the maximum depth  $D$ , we have succeeded in obtaining physically relevant results without resorting to hierarchy representations in nonstandard basis sets or using advanced DEOM propagation techniques. These could be exploited in further investigations of more realistic and challenging models, such as the multi-mode (instead of the single-mode) Brownian-oscillator model for the nonlocal interaction of the carrier with low-frequency intermolecular phonons or the explicit inclusion of the local interaction with high-frequency intramolecular vibrations.

## ACKNOWLEDGMENTS

This research was supported by the Science Fund of the Republic of Serbia, Grant No. 5468, Polaron Mobility in Model Systems and Real Materials–PolMoReMa. The author also acknowledges funding provided by the Institute of Physics Belgrade through a grant from the Ministry of Science, Technological Development, and Innovation of the Republic of Serbia. Numerical computations were performed on the PARADOX-IV supercomputing facility at the Scientific Computing Laboratory, National Center of Excellence for the Study of Complex Systems, Institute of Physics Belgrade. The author thanks Nenad Vukmirović for the careful reading of the manuscript.

## Appendix A: Coefficients $c_m$ and $\mu_m$ in Eq. (11) for the Brownian-oscillator spectral density

In Eq. (11), the terms with  $m = 0$  and 1 stem from the poles of  $\mathcal{J}(\omega)$  and read<sup>67,68</sup>

$$\mu_m = \gamma_0 + (-1)^m i\zeta, \quad (\text{A1})$$

$$c_m = (-1)^{m+1} \frac{E_0 \omega_0^2}{2\zeta} \left[ \coth\left(\frac{i\beta\mu_m}{2}\right) - 1 \right] \quad (\text{A2})$$

where

$$\zeta = \begin{cases} \sqrt{\omega_0^2 - \gamma_0^2}, & \gamma_0 < \omega_0 \\ i\sqrt{\gamma_0^2 - \omega_0^2}, & \gamma_0 > \omega_0. \end{cases} \quad (\text{A3})$$

The terms of Eq. (11) with  $m \geq 2$  are connected to the decomposition

$$\frac{1}{1 - e^{-z}} = \frac{1}{2} + \frac{1}{z} + \sum_{m=1}^{+\infty} \rho_m \left( \frac{1}{z - i\xi_m} + \frac{1}{z + i\xi_m} \right)$$

of the Bose–Einstein function in terms of its simple poles ( $0, \pm i\xi_m$ ) and residues ( $1, \rho_m$ ). Therefore, for  $m \geq 2$ ,<sup>67,68</sup>

$$\mu_m = \xi_{m-1} T, \quad (\text{A4})$$

$$\frac{c_m}{E_0 \omega_0} = \frac{-8\xi_{m-1}\rho_{m-1}(\beta\omega_0)(\beta\gamma_0)}{[(\beta\omega_0)^2 + \xi_{m-1}^2]^2 - 4\xi_{m-1}^2(\beta\gamma_0)^2}. \quad (\text{A5})$$

In the Matsubara decomposition,  $\xi_m = 2\pi m$ ,  $\rho_m = 1$ . In actual computations, we follow Ref. 101 and obtain  $\xi_m$  and  $\rho_m$  using the  $(N_{\text{BE}} - 1)/N_{\text{BE}}$  Padé approximant to the Bose–Einstein function.<sup>102,103</sup>

## Appendix B: Strong-damping limit

Here, we discuss the bath correlation function  $\mathcal{C}(t)$  in the strong-damping limit  $\gamma_0 \gg \omega_0$ . Equation (A1) determining the rates of the exponentials in Eq. (11) then becomes

$$\mu_0 \approx \frac{\omega_0^2}{2\gamma_0}, \quad \mu_1 \approx 2\gamma_0, \quad (\text{B1})$$

where we keep only the leading terms. The term  $e^{-\mu_0 t}$  tends to unity with increasing  $\gamma_0$ , which is a formal manifestation of the system gradually becoming similar to the statically disordered one, *vide infra*. Meanwhile, the term  $e^{-\mu_1 t}$  becomes increasingly similar to a (one-sided)  $\delta$  function, and the same holds for Matsubara terms at sufficiently high temperatures. In other words, in the strong-damping limit and at high temperatures,

$$\mathcal{C}(t) \approx c_0 + 2\Delta\delta(t), \quad (\text{B2})$$

where  $\Delta$  is given by Eq. (34) with  $K = 0$ . Using Eq. (A2) for  $m = 0$  and Eqs. (B1) and (34), and keeping only the leading-order terms, we recast Eq. (B2) as

$$\mathcal{C}(t) \approx 2E_0 T - \frac{4E_0 T}{\gamma_0} \delta(t). \quad (\text{B3})$$

By representing Gaussian static disorder in terms of appropriate bosonic operators, Ref. 104 formally establishes that quantum dynamics of a carrier in the bath defined by Eq. (B3) can be computed by averaging the dynamics modulated by the white noise in transfer integrals [the second term in Eq. (B3)] over different realizations of Gaussian static disorder in transfer integrals

[the first term in Eq. (B3)].  $\mathcal{C}(t)$  in Eq. (11) and its approximate version Eq. (B3) is the single-site bath correlation function, while nearest-neighbor transfer integrals are modulated by the difference between displacements of the corresponding local oscillators [Eq. (45)]. Therefore, the disorder strength is two times greater than in Eq. (B3), i.e.,  $\sigma^2 = 2 \times 2E_0T = 2\lambda JT$  [Eq. (8)], which coincides with Eq. (46). The white-noise term ensures that the long-time diffusion constant remains nonzero for large but finite  $\gamma_0$ , which is nowadays known as the environment-assisted (or noise-assisted) quantum transport.<sup>105–107</sup> The TLS avoids computing (and then averaging) noise-modulated dynamics in many static-disorder realizations by resorting to Eq. (44), which approximates noise effects through the exponential correction to the dynamics in the static landscape.

The approximation embodied in Eq. (44) provides the exact solution to white noise-modulated transport dynamics in the ordered Holstein model if we set  $\tau_d = \gamma_0/(2E_0T)$  and  $C_{jj}^{\text{dis}}(t) = 2J^2$ .<sup>107,108</sup> Although the exact solution to white noise-modulated transport dynamics in the ordered Peierls model is more complicated,<sup>108</sup> exponentially decaying terms  $\exp(-t/\tau_d)$  with  $\tau_d \propto \frac{\gamma_0}{E_0T}$  remain its distinctive feature. From that viewpoint, the TLS effectively assumes that the same exponentially decaying terms dominate  $C_{jj}(t)$  even in the statically disordered Peierls model with white noise. This suggests that  $\tau_d$  depends linearly on  $\gamma_0$  in the strong-damping limit.

### Appendix C: Coarse-grained nature of short-time dynamics for the Drude–Lorentz spectral density

Here, we explore how  $\text{Im } \mathcal{C}_{\text{DL}}(t=0) \neq 0$  yields problems with the equilibrium expectation value

$$\langle j_{\text{e-ph}}^2 \rangle = \sum_{\substack{q_2 \bar{m}_2 \\ q_1 \bar{m}_1}} \text{Tr}_S \{ J_{q_2} J_{q_1} \text{Tr}_B \{ f_2 f_1 \rho_{\text{tot}}^{\text{eq}} \} \}, \quad (\text{C1})$$

which should be purely real (and positive). In Eq. (C1) and in the following, we abbreviate  $f_{q_i m_i} \equiv f_i$ .

Using Eqs. (24) and (25), we evaluate  $\text{Tr}_B \{ f_2 f_1 \rho_{\text{tot}}^{\text{eq}} \}$  as

$$\begin{aligned} \text{Tr}_B \{ f_2 f_1 \rho_{\text{tot}}^{\text{eq}} \} &= \text{Tr}_B \left\{ F_{\mathbf{0}_2^+}^{(1)} f_1 \rho_{\text{tot}}^{\text{eq}} \right\} \\ &= \rho_{\mathbf{0}_{21}^+}^{(2,\text{eq})} + \delta_{m_1 \bar{m}_2} \eta_{q_2 q_1 \bar{m}_2} \rho_{\mathbf{0}}^{(0,\text{eq})}. \end{aligned} \quad (\text{C2})$$

Instead of Eq. (24), we could have used the generalized Wick's theorem in the form<sup>57,59</sup>

$$\begin{aligned} \text{Tr}_B \left\{ f_{qm} F_{\mathbf{n}}^{(n)} \rho_{\text{tot}}^{\text{eq}} \right\} &= \\ \rho_{\mathbf{n}_{qm}^+}^{(n+1,\text{eq})} &+ \sum_{q'm'} n_{q'm'} \langle f_{qm} f_{q'm'} \rangle_B^< \rho_{\mathbf{n}_{q'm'}^-}^{(n-1,\text{eq})}, \end{aligned} \quad (\text{C3})$$

with [see Eq. (13)]

$$\langle f_{qm} f_{q'm'} \rangle_B^< = \left\langle f_{qm}^{(I)}(0) f_{q'm'}^{(I)}(0_+) \right\rangle_B = \delta_{m \bar{m}'} \eta_{q' \bar{q}}^* \bar{q} \bar{m}', \quad (\text{C4})$$

to obtain

$$\begin{aligned} \text{Tr}_B \{ f_2 f_1 \rho_{\text{tot}}^{\text{eq}} \} &= \text{Tr}_B \left\{ f_2 F_{\mathbf{0}_1^+}^{(1)} \rho_{\text{tot}}^{\text{eq}} \right\} \\ &= \rho_{\mathbf{0}_{21}^+}^{(2,\text{eq})} + \delta_{m_1 \bar{m}_2} \eta_{q_2 \bar{q}_1}^* \bar{m}_2 \rho_{\mathbf{0}}^{(0,\text{eq})}. \end{aligned} \quad (\text{C5})$$

Inserting Eqs. (C2) or (C5) into Eq. (C1), and requiring that the two results for  $\langle j_{\text{e-ph}}^2 \rangle$  be identical, we obtain

$$\sum_{q_2 q_1 \bar{m}_2} (\eta_{q_2 q_1 \bar{m}_2} - \eta_{q_2 \bar{q}_1}^* \bar{m}_2) \text{Tr}_S \left\{ J_{q_2} J_{q_1} \rho_{\mathbf{0}}^{(0,\text{eq})} \right\} = 0. \quad (\text{C6})$$

Recalling that  $\eta_{q_2 q_1 \bar{m}_2} = \frac{\delta_{q_1 \bar{q}_2}}{N} c_{m_2}$ , we transform Eq. (C6) into

$$\sum_m (c_m - c_m^*) \sum_q \text{Tr}_S \left\{ J_q^\dagger J_q \rho_{\mathbf{0}}^{(0,\text{eq})} \right\} = 0. \quad (\text{C7})$$

To obtain the first factor of Eq. (C7), we perform the change of the dummy index  $\bar{m} \leftrightarrow m$ , which is permissible even for finite  $K$  because the truncated DEOM always includes pairs of complex-conjugated components. Each  $q$ -dependent term  $\text{Tr}_S \left\{ J_q^\dagger J_q \rho_{\mathbf{0}}^{(0,\text{eq})} \right\}$  is positive because  $\rho_{\mathbf{0}}^{(0,\text{eq})}$  is the equilibrium reduced density matrix, while the operator  $J_q^\dagger J_q$  is positive. We thus conclude that the two ways of evaluating  $\langle j_{\text{e-ph}}^2 \rangle$  yield the same result under the condition that

$$\sum_m \text{Im } c_m = 0. \quad (\text{C8})$$

While Eq. (C8) is satisfied for the BO SD, see Appendix A, for the DL SD we have

$$\sum_m \text{Im } c_m^{\text{DL}} = -E_0 \gamma_{\text{DL}} \neq 0. \quad (\text{C9})$$

This inconsistency of the DL model is resolved using Ishizaki's procedure.<sup>60</sup>



- <sup>1</sup>A. Troisi and G. Orlandi, "Charge-transport regime of crystalline organic semiconductors: Diffusion limited by thermal off-diagonal electronic disorder," *Phys. Rev. Lett.* **96**, 086601 (2006).
- <sup>2</sup>H. Sirringhaus, T. Sakanoue, and J.-F. Chang, "Charge-transport physics of high-mobility molecular semiconductors," *Phys. Status Solidi B* **249**, 1655–1676 (2012).
- <sup>3</sup>S. Fratini, D. Mayou, and S. Ciuchi, "The transient localization scenario for charge transport in crystalline organic materials," *Adv. Funct. Mater.* **26**, 2292–2315 (2016).
- <sup>4</sup>A. Y. Sosorov, D. R. Maslennikov, O. G. Kharlanov, I. Y. Chernyshov, V. V. Bruevich, and D. Y. Paraschuk, "Impact of low-frequency vibrations on charge transport in high-mobility organic semiconductors," *Phys. Status Solidi RRL* **13**, 1800485 (2019).
- <sup>5</sup>T. Nematirram and A. Troisi, "Modeling charge transport in high-mobility molecular semiconductors: Balancing electronic structure and quantum dynamics methods with the help of experiments," *J. Chem. Phys.* **152**, 190902 (2020).
- <sup>6</sup>S. Fratini, M. Nikolka, A. Salleo, G. Schweicher, and H. Sirringhaus, "Charge transport in high-mobility conjugated polymers and molecular semiconductors," *Nat. Mater.* **19**, 491–502 (2020).
- <sup>7</sup>B. M. T. C. Peluzo, R. Meena, L. Catalano, G. Schweicher, and M. T. Ruggiero, "Exploring the interplay of lattice dynamics and charge transport in organic semiconductors: Progress toward rational phonon engineering," *Angew. Chem. Int. Ed.* **64**, e202507566 (2025).
- <sup>8</sup>M. Fischer, M. Dressel, B. Gompf, A. K. Tripathi, and J. Pflaum, "Infrared spectroscopy on the charge accumulation layer in rubrene single crystals," *Appl. Phys. Lett.* **89**, 182103 (2006).
- <sup>9</sup>Z. Q. Li, V. Podzorov, N. Sai, M. C. Martin, M. E. Gershenson, M. Di Ventra, and D. N. Basov, "Light quasiparticles dominate electronic transport in molecular crystal field-effect transistors," *Phys. Rev. Lett.* **99**, 016403 (2007).
- <sup>10</sup>H. Yada, R. Uchida, H. Sekine, T. Terashige, S. Tao, Y. Matsui, N. Kida, S. Fratini, S. Ciuchi, Y. Okada, T. Uemura, J. Takeya, and H. Okamoto, "Carrier dynamics of rubrene single-crystals revealed by transient broadband terahertz spectroscopy," *Appl. Phys. Lett.* **105**, 143302 (2014).
- <sup>11</sup>H. Yada, H. Sekine, T. Miyamoto, T. Terashige, R. Uchida, T. Otaki, F. Maruike, N. Kida, T. Uemura, S. Watanabe, T. Okamoto, J. Takeya, and H. Okamoto, "Evaluating intrinsic mobility from transient terahertz conductivity spectra of microcrystal samples of organic molecular semiconductors," *Appl. Phys. Lett.* **115**, 143301 (2019).
- <sup>12</sup>Y. Han, T. Miyamoto, T. Otaki, N. Takamura, N. Kida, N. Osaka, J. Tsurumi, S. Watanabe, T. Okamoto, J. Takeya, and H. Okamoto, "Scattering mechanism of hole carriers in organic molecular semiconductors deduced from analyses of terahertz absorption spectra using Drude-Anderson model," *Appl. Phys. Lett.* **120**, 053302 (2022).
- <sup>13</sup>S. Giannini, L. Di Virgilio, M. Bardini, J. Hausch, J. J. Geuchies, W. Zheng, M. Volpi, J. Elsner, K. Broch, Y. H. Geerts, F. Schreiber, G. Schweicher, H. I. Wang, J. Blumberger, M. Bonn, and D. Beljonne, "Transiently delocalized states enhance hole mobility in organic molecular semiconductors," *Nat. Mater.* **22**, 1361–1369 (2023).
- <sup>14</sup>S. Fratini, S. Ciuchi, and D. Mayou, "Phenomenological model for charge dynamics and optical response of disordered systems: Application to organic semiconductors," *Phys. Rev. B* **89**, 235201 (2014).
- <sup>15</sup>S. Ciuchi, S. Fratini, and D. Mayou, "Transient localization in crystalline organic semiconductors," *Phys. Rev. B* **83**, 081202 (2011).
- <sup>16</sup>S. Ciuchi and S. Fratini, "Electronic transport and quantum localization effects in organic semiconductors," *Phys. Rev. B* **86**, 245201 (2012).
- <sup>17</sup>S. Fratini, S. Ciuchi, D. Mayou, G. T. de Laissardière, and A. Troisi, "A map of high-mobility molecular semiconductors," *Nat. Mater.* **16**, 998–1002 (2017).
- <sup>18</sup>T. Nematirram, S. Ciuchi, X. Xie, S. Fratini, and A. Troisi, "Practical computation of the charge mobility in molecular semiconductors using transient localization theory," *J. Phys. Chem. C* **123**, 6989–6997 (2019).
- <sup>19</sup>L. Wang, O. V. Prezhdo, and D. Beljonne, "Mixed quantum-classical dynamics for charge transport in organics," *Phys. Chem. Chem. Phys.* **17**, 12395–12406 (2015).
- <sup>20</sup>S. Giannini and J. Blumberger, "Charge transport in organic semiconductors: The perspective from nonadiabatic molecular dynamics," *Acc. Chem. Res.* **55**, 819–830 (2022).
- <sup>21</sup>J. E. Runeson, T. J. G. Drayton, and D. E. Manolopoulos, "Charge transport in organic semiconductors from the mapping approach to surface hopping," *J. Chem. Phys.* **161**, 144102 (2024).
- <sup>22</sup>A. Troisi and G. Orlandi, "Dynamics of the intermolecular transfer integral in crystalline organic semiconductors," *J. Phys. Chem. A* **110**, 4065–4070 (2006).
- <sup>23</sup>A. Troisi, "Prediction of the absolute charge mobility of molecular semiconductors: the case of rubrene," *Adv. Mater.* **19**, 2000–2004 (2007).
- <sup>24</sup>V. Janković, "Charge transport limited by nonlocal electron-phonon interaction. I. Hierarchical equations of motion approach," *Phys. Rev. B* **112**, 035111 (2025).
- <sup>25</sup>V. Janković, "Charge transport limited by nonlocal electron-phonon interaction. II. Numerically exact quantum dynamics in the slow-phonon regime," *Phys. Rev. B* **112**, 035112 (2025).
- <sup>26</sup>W. P. Su, J. R. Schrieffer, and A. J. Heeger, "Solitons in polyacetylene," *Phys. Rev. Lett.* **42**, 1698–1701 (1979).
- <sup>27</sup>M. Capone, W. Stephan, and M. Grilli, "Small-polaron formation and optical absorption in Su-Schrieffer-Heeger and Holstein models," *Phys. Rev. B* **56**, 4484–4493 (1997).
- <sup>28</sup>D. J. J. Marchand, G. De Filippis, V. Cataudella, M. Berciu, N. Nagaosa, N. V. Prokof'ev, A. S. Mishchenko, and P. C. E. Stamp, "Sharp Transition for Single Polarons in the One-Dimensional Su-Schrieffer-Heeger Model," *Phys. Rev. Lett.* **105**, 266605 (2010).
- <sup>29</sup>G. Schweicher, G. D'Avino, M. T. Ruggiero, D. J. Harkin, K. Broch, D. Venkateshvaran, G. Liu, A. Richard, C. Ruzié, J. Armstrong, A. R. Kennedy, K. Shankland, K. Takimiya, Y. H. Geerts, J. A. Zeitler, S. Fratini, and H. Sirringhaus, "Chasing the "killer" phonon mode for the rational design of low-disorder, high-mobility molecular semiconductors," *Adv. Mater.* **31**, 1902407 (2019).
- <sup>30</sup>A. Troisi, D. L. Cheung, and D. Andrienko, "Charge transport in semiconductors with multiscale conformational dynamics," *Phys. Rev. Lett.* **102**, 116602 (2009).
- <sup>31</sup>A. Troisi and D. L. Cheung, "Transition from dynamic to static disorder in one-dimensional organic semiconductors," *J. Chem. Phys.* **131**, 014703 (2009).
- <sup>32</sup>J. Kirkpatrick, V. Marcon, K. Kremer, J. Nelson, and D. Andrienko, "Columnar mesophases of hexabenzocoronene derivatives. II. Charge carrier mobility," *J. Chem. Phys.* **129**, 094506 (2008).
- <sup>33</sup>S. Mukamel, *Principles of Nonlinear Optical Spectroscopy* (Oxford University Press, Inc., New York, 1995).
- <sup>34</sup>L. Valkunas, D. Abramavicius, and T. Mančal, *Molecular Excitation Dynamics and Relaxation* (WILEY-VCH Verlag GmbH & Co. KGaA, 2013).
- <sup>35</sup>R. Feynman and F. Vernon, "The theory of a general quantum system interacting with a linear dissipative system," *Ann. Phys.* **24**, 118–173 (1963).
- <sup>36</sup>A. Garg, J. N. Onuchic, and V. Ambegaokar, "Effect of friction on electron transfer in biomolecules," *J. Chem. Phys.* **83**, 4491–4503 (1985).
- <sup>37</sup>A. J. Leggett, "Quantum tunneling in the presence of an arbitrary linear dissipation mechanism," *Phys. Rev. B* **30**, 1208–1218 (1984).
- <sup>38</sup>H.-P. Breuer and F. Petruccione, *The Theory of Open Quantum*



*Systems* (Oxford University Press, 2002).

- <sup>39</sup>U. Weiss, *Quantum Dissipative Systems*, 3rd ed. (WORLD SCIENTIFIC, 2008).
- <sup>40</sup>D. Wang, L. Chen, R. Zheng, L. Wang, and Q. Shi, "Communications: A nonperturbative quantum master equation approach to charge carrier transport in organic molecular crystals," *J. Chem. Phys.* **132**, 081101 (2010).
- <sup>41</sup>Y. Yan, M. Xu, Y. Liu, and Q. Shi, "Theoretical study of charge carrier transport in organic molecular crystals using the Nakajima-Zwanzig-Mori generalized master equation," *J. Chem. Phys.* **150**, 234101 (2019).
- <sup>42</sup>M. Lian, Y.-C. Wang, Y. Ke, and Y. Zhao, "Non-Markovian stochastic Schrödinger equation in k-space toward the calculation of carrier dynamics in organic semiconductors," *J. Chem. Phys.* **151**, 044115 (2019).
- <sup>43</sup>S. Bhattacharyya, T. Sayer, and A. Montoya-Castillo, "Anomalous transport of small polarons arises from transient lattice relaxation or immovable boundaries," *J. Phys. Chem. Lett.* **15**, 1382–1389 (2024).
- <sup>44</sup>L. Zhou, X. Gao, and Z. Shuai, "A stochastic Schrödinger equation and matrix product state approach to carrier transport in organic semiconductors with nonlocal electron-phonon interaction," *J. Chem. Phys.* **161**, 084118 (2024).
- <sup>45</sup>S. Bhattacharyya, T. Sayer, and A. Montoya-Castillo, "Mori generalized master equations offer an efficient route to predict and interpret polaron transport," *Chem. Sci.* **15**, 16715–16723 (2024).
- <sup>46</sup>S. Bhattacharyya, T. Sayer, and A. Montoya-Castillo, "Nonequilibrium relaxation exponentially delays the onset of quantum diffusion," *Proc. Natl. Acad. Sci.* **122**, e2424582122 (2025).
- <sup>47</sup>G. Mahan, *Many-Particle Physics* (Kluwer Academic, New York, 2000).
- <sup>48</sup>R. Kubo, M. Toda, and N. Hashitsume, *Statistical Physics II: Nonequilibrium Statistical Mechanics* (Springer-Verlag Berlin Heidelberg, 1985).
- <sup>49</sup>L. Song and Q. Shi, "A new approach to calculate charge carrier transport mobility in organic molecular crystals from imaginary time path integral simulations," *J. Chem. Phys.* **142**, 174103 (2015).
- <sup>50</sup>T. Xing, T. Li, Y. Yan, S. Bai, and Q. Shi, "Application of the imaginary time hierarchical equations of motion method to calculate real time correlation functions," *J. Chem. Phys.* **156**, 244102 (2022).
- <sup>51</sup>H. Takahashi and R. Borrelli, "Tensor-Train Format Hierarchical Equations of Motion Formalism: Charge Transfer in Organic Semiconductors via Dissipative Holstein Models," *J. Chem. Theory Comput.* **20**, 7052–7064 (2024).
- <sup>52</sup>P. Gosar and S.-i. Choi, "Linear-response theory of the electron mobility in molecular crystals," *Phys. Rev.* **150**, 529–538 (1966).
- <sup>53</sup>P. Gosar and I. Vilfan, "Phonon-assisted current in organic molecular crystals," *Mol. Phys.* **18**, 49–61 (1970).
- <sup>54</sup>K. Hannebald and P. A. Bobbert, "Anisotropy effects in phonon-assisted charge-carrier transport in organic molecular crystals," *Phys. Rev. B* **69**, 075212 (2004).
- <sup>55</sup>Y. Yan, "Theory of open quantum systems with bath of electrons and phonons and spins: Many-dissipaton density matrixes approach," *J. Chem. Phys.* **140**, 054105 (2014).
- <sup>56</sup>Y. Yan, J. Jin, R.-X. Xu, and X. Zheng, "Dissipation equation of motion approach to open quantum systems," *Front. Phys.* **11**, 110306 (2016).
- <sup>57</sup>H.-D. Zhang, R.-X. Xu, X. Zheng, and Y. Yan, "Statistical quasi-particle theory for open quantum systems," *Mol. Phys.* **116**, 780–812 (2018).
- <sup>58</sup>Y. Wang, Z. J. Pan, H.-D. Zhang, and Y. J. Yan, "Dissipation dynamics theory versus quantum master equations," *Chem. Phys.* **515**, 94–101 (2018).
- <sup>59</sup>Y. Wang and Y. Yan, "Quantum mechanics of open systems: Dissipaton theories," *J. Chem. Phys.* **157**, 170901 (2022).
- <sup>60</sup>A. Ishizaki, "Prerequisites for relevant spectral density and convergence of reduced density matrices at low temperatures," *J. Phys. Soc. Jpn.* **89**, 015001 (2020).
- <sup>61</sup>T. Li, Y. Yan, and Q. Shi, "A low-temperature quantum Fokker-Planck equation that improves the numerical stability of the hierarchical equations of motion for the Brownian oscillator spectral density," *J. Chem. Phys.* **156**, 064107 (2022).
- <sup>62</sup>V. Janković, "Holstein polaron transport from numerically "exact" real-time quantum dynamics simulations," *J. Chem. Phys.* **159**, 094113 (2023).
- <sup>63</sup>Y. Zhao, D. W. Brown, and K. Lindenberg, "On the Munn-Silbey approach to nonlocal exciton-phonon coupling," *J. Chem. Phys.* **100**, 2335–2345 (1994).
- <sup>64</sup>M. Tanaka and Y. Tanimura, "Quantum dissipative dynamics of electron transfer reaction system: Nonperturbative hierarchy equations approach," *J. Phys. Soc. Jpn.* **78**, 073802 (2009).
- <sup>65</sup>M. Tanaka and Y. Tanimura, "Multistate electron transfer dynamics in the condensed phase: Exact calculations from the reduced hierarchy equations of motion approach," *J. Chem. Phys.* **132**, 214502 (2010).
- <sup>66</sup>J. Roden, W. T. Strunz, K. B. Whaley, and A. Eisfeld, "Accounting for intra-molecular vibrational modes in open quantum system description of molecular systems," *J. Chem. Phys.* **137**, 204110 (2012).
- <sup>67</sup>D. I. G. Bennett, P. Malý, C. Kreisbeck, R. van Grondelle, and A. Aspuru-Guzik, "Mechanistic regimes of vibronic transport in a heterodimer and the design principle of incoherent vibronic transport in phycobiliproteins," *J. Phys. Chem. Lett.* **9**, 2665–2670 (2018).
- <sup>68</sup>T. Li, Y. Yan, and Q. Shi, "Is there a finite mobility for the one vibrational mode Holstein model? Implications from real time simulations," *J. Chem. Phys.* **160**, 111102 (2024).
- <sup>69</sup>Y. Yan and R. X. Xu, "Quantum mechanics of dissipative systems," *Annu. Rev. Phys. Chem.* **56**, 187–219 (2005).
- <sup>70</sup>J.-J. Ding, R.-X. Xu, and Y. Yan, "Optimizing hierarchical equations of motion for quantum dissipation and quantifying quantum bath effects on quantum transfer mechanisms," *J. Chem. Phys.* **136**, 224103 (2012).
- <sup>71</sup>H.-D. Zhang, Q. Qiao, R.-X. Xu, and Y. Yan, "Effects of Herzberg-Teller vibronic coupling on coherent excitation energy transfer," *J. Chem. Phys.* **145**, 204109 (2016).
- <sup>72</sup>H.-D. Zhang, R.-X. Xu, X. Zheng, and Y. Yan, "Nonperturbative spin-boson and spin-spin dynamics and nonlinear Fano interferences: A unified dissipation theory based study," *J. Chem. Phys.* **142**, 024112 (2015).
- <sup>73</sup>Z.-H. Chen, Y. Wang, R.-X. Xu, and Y. Yan, "Correlated vibration—solvent effects on the non-Condon exciton spectroscopy," *J. Chem. Phys.* **154**, 244105 (2021).
- <sup>74</sup>Y. Su, Y. Wang, and W. Dou, "Nonperturbative open quantum dynamics bypass influence functional," (2025), arXiv:2503.00297 [quant-ph].
- <sup>75</sup>H. Gong, Y. Wang, H.-D. Zhang, Q. Qiao, R.-X. Xu, X. Zheng, and Y. Yan, "Equilibrium and transient thermodynamics: A unified dissipation-space approach," *J. Chem. Phys.* **153**, 154111 (2020).
- <sup>76</sup>D. P. McMahon and A. Troisi, "Organic semiconductors: Impact of disorder at different timescales," *ChemPhysChem* **11**, 2067–2074 (2010).
- <sup>77</sup>X. Cui, Y. Yan, and J. Wei, "Theoretical study on the effect of environment on excitation energy transfer in photosynthetic light-harvesting systems," *J. Phys. Chem. B* **124**, 2354–2362 (2020).
- <sup>78</sup>X. Cui, Y. Yan, and J. Wei, "Role of Pigment-Protein Coupling in the Energy Transport Dynamics in the Fenna-Matthews-Olson Complex," *J. Phys. Chem. B* **125**, 11884–11892 (2021).
- <sup>79</sup>J. Fang, Z.-H. Chen, Y. Su, Z.-F. Zhu, Y. Wang, R.-X. Xu, and Y. Yan, "Coherent excitation energy transfer in model photosynthetic reaction center: Effects of non-Markovian quantum environment," *J. Chem. Phys.* **157**, 084119 (2022).
- <sup>80</sup>X. Cui, Y. Yan, and J. Wei, "Theoretical Study

- on the Excitation Energy Transfer Dynamics in the Phycoerythrin PE555 Light-Harvesting Complex,” *ACS Omega* **9**, 51228–51236 (2024).
- <sup>81</sup>D. Hou, S. Wang, R. Wang, L. Z. Ye, R. X. Xu, X. Zheng, and Y. J. Yan, “Improving the efficiency of hierarchical equations of motion approach and application to coherent dynamics in Aharonov–Bohm interferometers,” *J. Chem. Phys.* **142**, 104112 (2015).
- <sup>82</sup>Y. Kong, H.-D. Zhang, Y.-M. Wang, R.-X. Xu, and Y. Yan, “Dissipaton equation of motion with controlled truncation,” *Chin. J. Chem. Phys.* **28**, 409–414 (2015).
- <sup>83</sup>A. Ishizaki and Y. Tanimura, “Quantum dynamics of system strongly coupled to low-temperature colored noise bath: Reduced hierarchy equations approach,” *J. Phys. Soc. Jpn.* **74**, 3131–3134 (2005).
- <sup>84</sup>Q. Shi, L. Chen, G. Nan, R.-X. Xu, and Y. Yan, “Efficient hierarchical liouville space propagator to quantum dissipative dynamics,” *J. Chem. Phys.* **130**, 084105 (2009).
- <sup>85</sup>I. S. Dunn, R. Tempelaar, and D. R. Reichman, “Removing instabilities in the hierarchical equations of motion: Exact and approximate projection approaches,” *J. Chem. Phys.* **150**, 184109 (2019).
- <sup>86</sup>T. P. Fay, “A simple improved low temperature correction for the hierarchical equations of motion,” *J. Chem. Phys.* **157**, 054108 (2022).
- <sup>87</sup>J. Strümpfer and K. Schulten, “Open quantum dynamics calculations with the hierarchy equations of motion on parallel computers,” *J. Chem. Theory Comput.* **8**, 2808–2816 (2012).
- <sup>88</sup>V. Janković and N. Vukmirović, “Spectral and thermodynamic properties of the Holstein polaron: Hierarchical equations of motion approach,” *Phys. Rev. B* **105**, 054311 (2022).
- <sup>89</sup>H.-D. Zhang, Q. Qiao, R.-X. Xu, X. Zheng, and Y. Yan, “Efficient steady-state solver for hierarchical quantum master equations,” *J. Chem. Phys.* **147**, 044105 (2017).
- <sup>90</sup>P. Mitrić, “Dynamical quantum typicality: Simple method for investigating transport properties applied to the Holstein model,” *Phys. Rev. B* **111**, 195140 (2025).
- <sup>91</sup>P. Mitrić, V. Dobrosavljević, and D. Tanasković, “Precursors to anderson localization in the holstein model: Quantum and quantum-classical solutions,” *Phys. Rev. B* **111**, L161105 (2025).
- <sup>92</sup>J. H. Fetherolf, D. Golež, and T. C. Berkelbach, “A unification of the holstein polaron and dynamic disorder pictures of charge transport in organic crystals,” *Phys. Rev. X* **10**, 021062 (2020).
- <sup>93</sup>J. H. Fetherolf, P. Shih, and T. C. Berkelbach, “Conductivity of an electron coupled to anharmonic phonons: Quantum-classical simulations and comparison of approximations,” *Phys. Rev. B* **107**, 064304 (2023).
- <sup>94</sup>P. W. Anderson, “Absence of diffusion in certain random lattices,” *Phys. Rev.* **109**, 1492–1505 (1958).
- <sup>95</sup>S. Fratini and S. Ciuchi, “Dynamical localization corrections to band transport,” *Phys. Rev. Res.* **2**, 013001 (2020).
- <sup>96</sup>H. Rammal, A. Ralko, S. Ciuchi, and S. Fratini, “Transient localization from the interaction with quantum bosons,” *Phys. Rev. Lett.* **132**, 266502 (2024).
- <sup>97</sup>V. Podzorov, E. Menard, A. Borissov, V. Kiryukhin, J. A. Rogers, and M. E. Gershenson, “Intrinsic charge transport on the surface of organic semiconductors,” *Phys. Rev. Lett.* **93**, 086602 (2004).
- <sup>98</sup>V. Podzorov, E. Menard, J. A. Rogers, and M. E. Gershenson, “Hall effect in the accumulation layers on the surface of organic semiconductors,” *Phys. Rev. Lett.* **95**, 226601 (2005).
- <sup>99</sup>J. Takeya, J. Kato, K. Hara, M. Yamagishi, R. Hirahara, K. Yamada, Y. Nakazawa, S. Ikehata, K. Tsukagoshi, Y. Aoyagi, T. Takenobu, and Y. Iwasa, “In-crystal and surface charge transport of electric-field-induced carriers in organic single-crystal semiconductors,” *Phys. Rev. Lett.* **98**, 196804 (2007).
- <sup>100</sup>A. Ishizaki and G. R. Fleming, “Unified treatment of quantum coherent and incoherent hopping dynamics in electronic energy transfer: Reduced hierarchy equation approach,” *J. Chem. Phys.* **130**, 234111 (2009).
- <sup>101</sup>G. Ritschel and A. Eisfeld, “Analytic representations of bath correlation functions for ohmic and superohmic spectral densities using simple poles,” *J. Chem. Phys.* **141**, 094101 (2014).
- <sup>102</sup>J. Hu, R.-X. Xu, and Y. Yan, “Communication: Padé spectrum decomposition of Fermi function and Bose function,” *J. Chem. Phys.* **133**, 101106 (2010).
- <sup>103</sup>J. Hu, M. Luo, F. Jiang, R.-X. Xu, and Y. Yan, “Padé spectrum decompositions of quantum distribution functions and optimal hierarchical equations of motion construction for quantum open systems,” *J. Chem. Phys.* **134**, 244106 (2011).
- <sup>104</sup>M. F. Gelin, A. Velardo, and R. Borrelli, “Efficient quantum dynamics simulations of complex molecular systems: A unified treatment of dynamic and static disorder,” *J. Chem. Phys.* **155**, 134102 (2021).
- <sup>105</sup>P. Rebentrost, M. Mohseni, I. Kassal, S. Lloyd, and A. Aspuru-Guzik, “Environment-assisted quantum transport,” *New J. Phys.* **11**, 033003 (2009).
- <sup>106</sup>F. Caruso, A. W. Chin, A. Datta, S. F. Huelga, and M. B. Plenio, “Highly efficient energy excitation transfer in light-harvesting complexes: The fundamental role of noise-assisted transport,” *J. Chem. Phys.* **131**, 105106 (2009).
- <sup>107</sup>J. M. Moix, M. Khasin, and J. Cao, “Coherent quantum transport in disordered systems: I. The influence of dephasing on the transport properties and absorption spectra on one-dimensional systems,” *New J. Phys.* **15**, 085010 (2013).
- <sup>108</sup>A. Madhukar and W. Post, “Exact solution for the diffusion of a particle in a medium with site diagonal and off-diagonal dynamic disorder,” *Phys. Rev. Lett.* **39**, 1424–1427 (1977).